DEVELOPMENT AND CONTROL OF A FLEXIBLE ACTUATION-BASED DELTA ROBOT

by

Yasiru Suharshana Fernando

A Thesis Submitted in Partial Fulfillment of the Requirements for the Degree of Master of Engineering in Mechatronics

Examination Committee: Prof. Manukid Parnichkun (Chairperson)
Dr. Mongkol Ekpanyapong
Dr. Tanujjal Bora

Nationality: Sri Lankan
Previous Degree: Bachelor of Science in Mechanical Engineering
Sri Lanka Institute of Information Technology
Malabe, Sri Lanka

Scholarship Donor: AITAA Sri Lanka Chapter - AIT Scholarships

Asian Institute of Technology
School of Engineering and Technology
Thailand
May 2022

AUTHOR'S DECLARATION

I, Yasiru Suharshana Fernando, declare that the research work carried out for this thesis was in accordance with the regulations of the Asian Institute of Technology. The work presented in it are my own and has been generated by me as the result of my own original research, and if external sources were used, such sources have been cited. It is original and has not been submitted to any other institution to obtain another degree or qualification. This is a true copy of the thesis, including final revisions.

Date: 10th May 2022

Nam: Yasiru Suharshana Fernando

Signature:

ACKNOWLEDGMENTS

I would like to express my appreciation and gratitude to my advisor Prof. Manukid Parnichkun for the valuable guidance, ideas and support extended towards the successful completion of this thesis. It would have been difficult to complete this thesis without his advice.

Furthermore, it was a great pleasure to have Dr. Mongkol Ekpanyapong and Dr. Tanujjal Bora as examination committee members for their insightful remarks and suggestions.

In addition, I would like to extend my thanks to Mr. Hoang Hung Manh for aiding and supporting the laboratory work required for this thesis.

I would also like to thank AIT and AIT Alumni Association Sri Lanka Chapter for providing me with the scholarships that enabled me to pursue my Master's degree.

Finally, I would like to thank my parents, family and friends for their unwavering support and encouragement to fulfill my educational goals.

ABSTRACT

Soft Robotics is a novel branch of Robotics that has emerged in the recent past. The utilization of soft materials rather than traditional rigid materials has allowed the operation of these robots to become safer and more human centered. This thesis aims to develop a Delta Robot with flexible actuation to further the research carried out for soft robotic development. To obtain Delta Robot like behaviour which requires extension of the actuator, the Reverse Pneumatic Artificial Muscle (RPAM) was used in this thesis as the type of flexible actuator. Developed with latex rubber tubes and inextensible fiber wrappings, this type of actuator has a high pressure to length increment ratio and is convenient to be fabricated. Furthermore, as compared to other types of flexible actuators, the RPAM provides a nearly linear relationship between pressure and strain. The robot developed in this thesis utilizes three RPAM actuators powered by compressed air to achieve a hemispherical space of radius 12.37cm and variation angle of 31^{o}. PID control was used to regulate the actuation profiles of the solenoid valves which regulates the pressure within the actuators. Through the use of a Look-Up Table, the robot can be commanded to move to a pre-recorded position to successfully perform pick and place operations.

Keywords: Flexible Actuator, Delta Robot, Reverse Pneumatic Artificial Muscle

CONTENTS

CONTENTS

LIST OF TABLES

LIST OF FIGURES

LIST OF FIGURES

LIST OF FIGURES

LIST OF ABBREVIATIONS

PAM = Pneumatic Artificial Muscle
RPAM = Reverse Pneumatic Artificial Muscle
SH = Soft Healing
PPAM = Pleated Pneumatic Artificial Muscle
PID = Proportional Integral Derivative
SMC = Sliding Mode Controller
MDP = Markov Decision Process
LSTM = Long Short-Term Memory
MLP = Multi-Layer Perceptron
ANN = Artificial Neural Network
PLA = Poly-Lactic Acid
CAD = Computer Aided Design
ADC = Analog to Digital Converter
LUT = Look-Up Table
DOF = Degree Of Freedom
IMU = Inertial Measurement Unit

CHAPTER 1
INTRODUCTION

1.1 Background of the Study

Amongst the many varieties of industrial robots, Delta robots are fast with great precision and are typically utilized in the pharmaceutical and electronic industry. The linkages for Delta robots are configured parallelly which provide the dexterity to perform the fast pick and place tasks. However, these types of robots are confined to a limited working envelope.

In the recent past, researchers have strived to incorporate softer materials for robot bodies paving the way for Soft Robotics. Soft robots are the type of robots that utilize soft and compliant materials along with suitable actuation techniques to provide delicate motions and manipulations. Soft robots are known to be adaptations of nature's most versatile creatures. Elephant trunks, snakes, jellyfish, and octopi are a few inspirations behind the designs of soft robots.

Soft robots are most commonly developed with silicone-based materials with pneumatic actuation. Thereby, the soft robots are generally safe to be used around humans as the risk from impacts are much less compared to rigid robots made of metallic materials. Certain configurations of soft robots can be developed such that they could be manipulated in constrained environments.

1.2 Statement of the Problem

Soft robots are fabricated and operated differently as compared to traditional robots. Due to the use of power sources such as pneumatics, controlling the soft robot is more difficult. Furthermore, they require specialized methods of feedback along with advanced control mechanisms. Therefore, it is necessary to implement and experiment with soft robotics to innovate effective control techniques.

Serial link robots made with rigid materials can be easily manipulated. This is mainly due to the rigidity and strength of materials as well as the power of actuators used. As mentioned in the previous section, soft robots do not have strong bodies or powerful actuators. Thereby, it is difficult for soft robots to successfully operate with serial linkages.

In order to implement a successful soft robot, the structure should be built with a closed chain i.e., parallel robot. This configuration maybe beneficial to the soft robot to maintain its rigidity and provide powerful actuation.

1.3 Objectives of the Study

This research aims to develop a parallel robot in the form of a Delta Robot with soft actuators.

1. Develop a 3 degree of freedom Delta Robot with soft pneumatic actuators.
2. Design and fabricate artificial pneumatic muscles which can either bend or change its length.
3. Using an appropriate feedback mechanism, implement an advanced controller for position control of the robot.

1.4 Scope and Limitations

The scope of this thesis is as follows:

1. Develop 3 bellow type pneumatic muscles to enable 3 degrees of freedom.
2. Control the robot in translational x-y-z planes.
3. Use pressure sensors for feedback.
4. The robot is planned to have a working environment of a hemisphere of radius 5cm with variation angle of 15^{o}.

1.5 Contribution

The following contributions are to be expected through this research:

- Delta robots are generally built with rigid materials. This research aims to develop a delta type robot with soft and compliant materials. Such a configuration can be a novel research interest in the field of soft robotics.
- This parallel robot configuration will be actuated through pneumatics.

1.6 Organization of the Study

The remainder of this thesis is organized as follows. Chapter one provides a literature review which discusses previous work done by researchers that is useful to develop this thesis. Chapter three describes the processes and methods used to develop this thesis. Chapter four analyses the results obtained throughout this thesis. Chapter five concludes this thesis along with suggestions for future work.

CHAPTER 2
LITERATURE REVIEW

Chapter 2 describes the techniques and types of mechanism that are used in this thesis and other related work. The first part is a brief overview on Delta robots followed by an analysis of several types of Soft Actuators. The next subsection reviews various types of actuation and feedback mechanisms while the final section reviews control structures used in developing soft robots.

2.1 Delta Robots

Poppeová Viera et al. (2011) describes the Delta robot as a parallel robot which includes parallelogram shaped output links connected to input link rods which are actuated through rotational or linear actuators. By using three of such parallelograms, the orientation of the end effector is restricted allowing only three purely translational degrees of freedom as shown in Figure 2.1. Due to the low mass of the links, the robot consists of low inertia resulting in higher accelerations. According to the authors, Delta Robots are best suited for high-speed pick and place operations involving lightweight payloads.

Figure 2.1

Delta Robot Parts

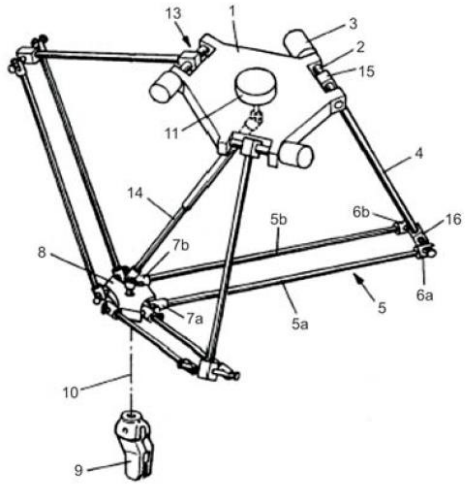

1 - Base element
2 - Shaft
3 - Fixed parts
4 - Arm
5a, 5b - Linking bars
6a, 6b - Revolute joints
7a, 7b - Revolute joints
8 - Movable element
9 - Working element
10 - End-effector joint
11 - Fixed motor
12 - Control system
13 - Actuator
14 - Telescopic arm (optional)
15 - First extremity
16 - Second extremity

Jayant Patil SSBT & P Deshmukh (2015.) proposes a control scheme for a Delta Robot with a control unit and image processing. The authors also provide a comparison on Serial versus Delta Robots as shown in Table 2.1.

Table 2.1

Serial vs Delta Comparison

Feature	**Serial Robot**	**Parallel Robot**
Inverse Kinematics	Easy	Very Difficult
Position Error	Accumulates	Averages
Stiffness	Low	High
Accuracy	Low	High
Dynamic Characteristics	Poor	High

The proposed system utilized a camera for visual feedback and a MATLAB program was used to calculate inverse kinematics from a reference position.

Delta Robots are widely available in the market. Brands such as FANUC, ABB and BOSCH. They are mostly used for low payload applications, particularly pick and place. Therefore, Delta Robots are highly versatile in the electronics, pharmaceutical and packaging industries. Delta Robots have recently been used as 3D printers(Hsieh, 2017).

Blumenschein Laura H. & Meng¨uc Yigit (2019) developed a delta mechanism with soft actuators. The soft bellows of the actuators have been 3D printed with the rubber like material Agilus while the surrounding support material are 3D printed ABS plastic. The authors have tested various types of soft bellow configurations which is capable of different types of motions as shown in Figure 2.2. Furthermore, the authors used a collection of soft delta mechanisms distributed in a larger locomotion robot which moves similar to a starfish.

Figure 2.2

Designs for collective actuation concept

2.2 Soft Actuators

2.2.1 Pneumatic Artificial Muscle (PAM)

McKibben actuators are a type of Pneumatic Artificial Muscle (PAM) which provides translational motion through extension or contraction of the muscle. They are usually made of an elastic tubing wrapped with a meshed sheath. One end is sealed while the other is supplied compressed air. When air is supplied, the tube expands, and the expansion is restricted by the sheath. Thereby, the muscle expands laterally rather than longitudinally as depicted in Figure 2.3.

Andrikopoulos et al, (2013) develops a switching Model Predictive Control technique for PAMs. In this case, the authors developed the dynamic model for the PAM. Soft robots are often associated with non-linearities due to the use of compliant materials which require elastic deformation for actuation. To manage the non-linearities, the author has utilized Piece-Wise Affine system model approximation.

Figure 2.3

Simplified Geometrical Model of PAM a)relaxed and b)inflated

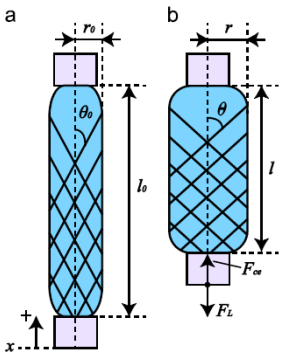

Hošovský et al., (2016) utilizes an antagonistic PAM system which provides rotary motion for a 2 degree of freedom serial robot. This arrangement mimics the action of biceps and triceps of the human arm. The dynamics of the robot have been derived through Lagrangian mechanics with certain parameters and the pneumatic muscle force function being derived through experimental means. This type of mechanism has been proven to be beneficial in developing soft rehabilitation robots (Liu et al., 2020).

Figure 2.4

a) Planar Robotic Arm with PAM b) Lagrangian Formulation

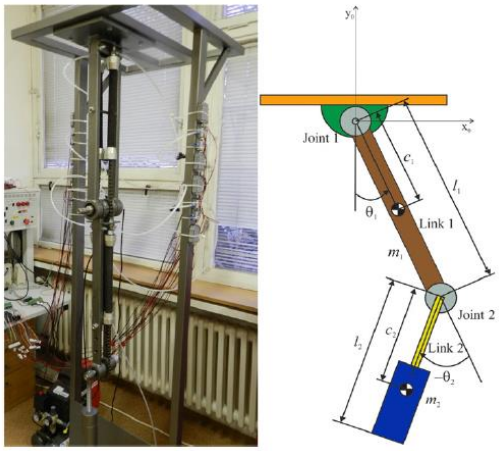

Kadowaki et al., (2021) proposes improvements for McKibben actuators based on end shape deformation. In this paper, the authors factor in the rounded shape of the end of the actuators when modelling the McKibben actuator. This provided increased accuracy of the proposed model against the previous model as compared with the measured results.

Wang & Xu (2021) developed a soft parallel robot based on pneumatic artificial muscles for wrist rehabilitation. This setup is useful for recovering post-stroke and post-surgery patients. The aim of this particular research is to develop a platform which can be teleoperated and doesn't require a doctor or a physiotherapist to be present with the patient during the treatment. The soft robot consists of 3 rotational degrees of freedom and is similar to the structure of a Stewart-Gough platform. The system utilized EMG sensors for feedback.

Figure 2.5

Wrist Rehabilitation Robot

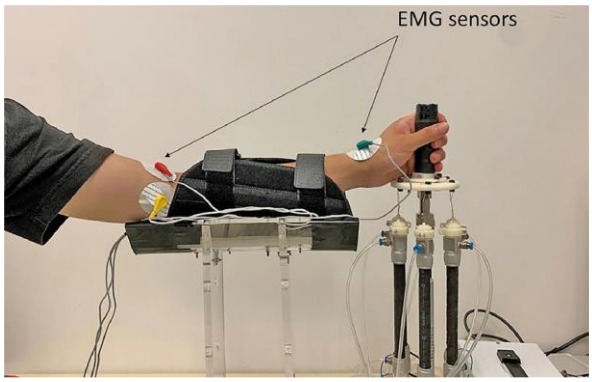

2.2.2 Reverse Pneumatic Artificial Muscles

Reverse Pneumatic Artificial Muscles (RPAMs) operate with the same principles as a Pneumatic Artificial Muscle (PAM). However, the arrangement of the restricting fibers alters the resulting motion. The meshed fibers of PAMs restrict motion mostly in the longitudinal direction. In the case of an RPAM, the fibers are arranged in a helical pattern. This provides a ring-like restriction for radial expansion while allowing longitudinal expansion.

Hawkes et al. (2016) implemented such an actuator which can achieve 300% strain as depicted in figure 2.6. Compared to a PAM, which can shorten by a small length upon actuation, this type of actuator can linearly elongate to great lengths. Thereby, it has the potential to be utilized in a Delta Robot configuration with a wider working space. In addition, this type of actuator is convenient to fabricate with latex rubber tubes for the body and a strong type of thread for the fiber.

Skorina et al. (2015) utilized the same concept with a silicone molded actuator. This custom designed actuator has a better advantage over the latex tube as it has uniformly spaced double helix fiber wrapping, whereas the latex tube wrapping is non-uniform. Skorina et al. (2016) later utilized these types of actuators to develop a modular manipulator with 2 DoF universal joint actuated by 3 RPAMs as shown in figure 2.7.

Figure 2.6

Reverse Pneumatic Artificial Muscle (RPAM)

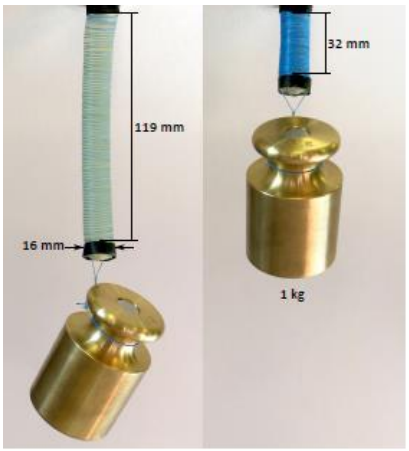

Figure 2.7

RPAM and the Modular Manipulator

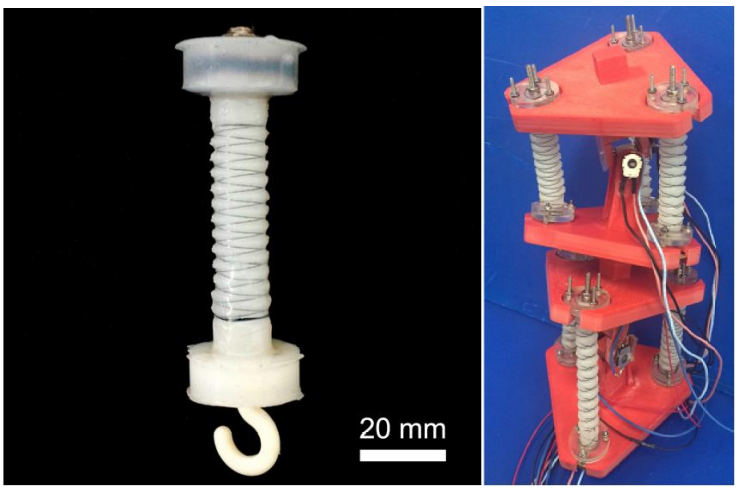

Furthermore, these types of actuators have the advantage of being programmed mechanically. The pattern and arrangement of the fibers can allow the actuator to expand, extend and twist (Connolly et al., 2015). The different functionalities of these actuators can be combined within a manipulator which provides greater dexterity to perform tasks (Al-Ibadi et al., 2018).

2.2.3 Molded Actuators

One advantage of soft robots is the ability to customize the actuators as needed. They can be fabricated to any shape and size desired as long as it can be molded with a suitable mold and elastomeric material. One such actuator can is the Pneu-Net actuator

which contains air chambers along the length of its body. When supplied with air, the chambers expand bending the body as in Figure 2.8.

Sun et al. (2020) developed a variation of the Pneu-Net actuator with a toothed configuration that mimics pangolin scales. This arrangement provided enhanced stiffness for the gripper mechanism they developed. T. Wang et al.(2018) proposes a Pneu-Net actuator with the oblique chambers slanted at an angle. The authors have conducted Finite Element Analysis on different oblique angles and similar boundary conditions.

It is widely accepted that Pneu-Net type actuators are ideal for bending motions. Hence, they most prominently used in gripper mechanisms as depicted in figure 2.8.

Figure 2.8

Bending Soft Actuators in Grippers

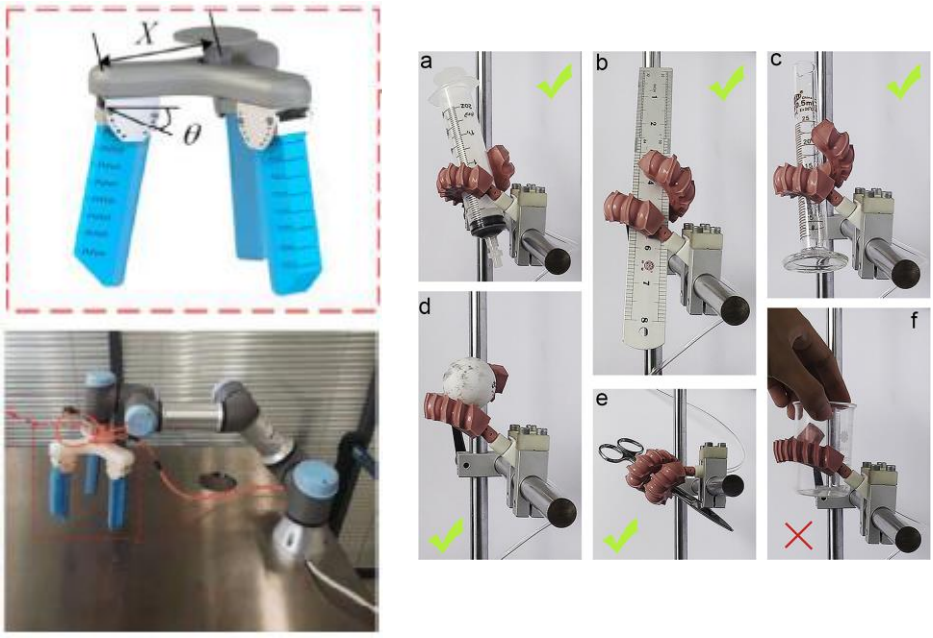

The Pneu-Net actuators are akin to fingers, and it is necessary to use several actuators in parallel to gain advantage of them. There are several other types of molded elastomeric actuators which can be utilized as complete manipulators. Marchese & Rus (2016) have developed a segmented soft continuum arm robot. The design is modular, and each segment contains four chambers that span along the length of the segment.

The manipulator can be positioned anywhere on its working envelope depending on the airflow into the chambers and the combination of chambers. The outcome of this manipulator is very similar to the operation of an elephant's trunk. In order to control the air pressure in each chamber, the authors have utilized 16 high-capacity fluidic drive cylinders. This mechanism uses a piston setup driven through linear drives.

Figure 2.9

Soft Fluidic Elastomer Manipulator

2.2.4 Materials

Soft robots can be developed in many ways using a variety of materials. Soft actuators are mostly fabricated with elastomeric substances such as silicone and actuated with pneumatics. The McKibben type actuators discussed previously utilize materials available in the market and the fabrication process is rather simple. The molded actuators require some effort as it is necessary to design and fabricate a precise mold. Certain researchers have utilized 3D printing process to fabricate actuators to obtain similar results (He et al., 2021). Other researchers have utilized fabric materials to increase strength and stiffness (Khin et al., 2017).

Terryn et al. (2021) reviews on utilizing self-healing polymers for soft robotics. The author describes how soft materials can be resilient and adaptive to the environment as

well as the susceptibility of the materials to damage, cuts and tears from sharp objects. Figure 2.10 depicts the different types of damage that can be inflicted on soft robotic materials.

Figure 2.10

Damaging Modes for Soft Robotics in Unstructured and Dynamic Environments

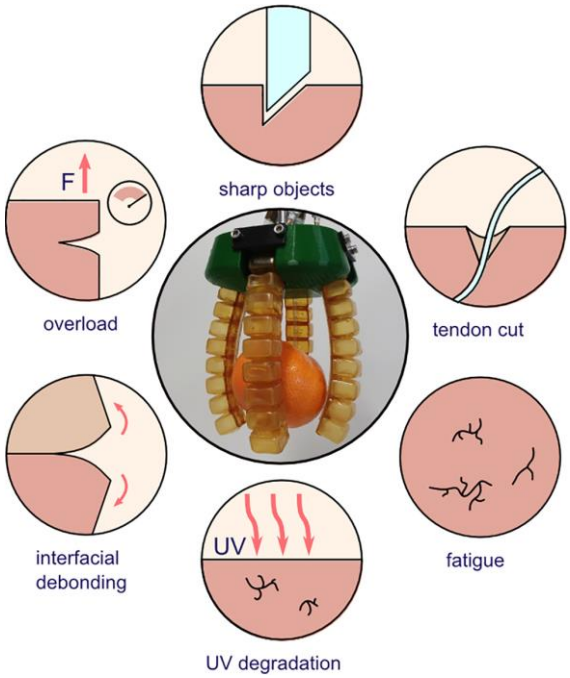

Terryn et al. (2017) provides in-depth information about the materials and experiments on the Soft Healing (SH) polymers developed for soft robots. The actuators were developed as SH Pleated Pneumatic Artificial Muscles (PPAM) which is similar to the Pneu-Nets actuators discussed in the previous sub-sections. The material used for the SH polymer is based on reversible Diels-Alder bond reaction between diene (furan) and dienophile (maleimide). Figure 2.11 depicts the process at which the polymer performs the self-healing actions where the cut surface at room temperature (25^{o}C) is heated to 80^{o}C and cooled back to room temperature.

Figure 2.11

Schematic of the SH cycle of DA Polymers.

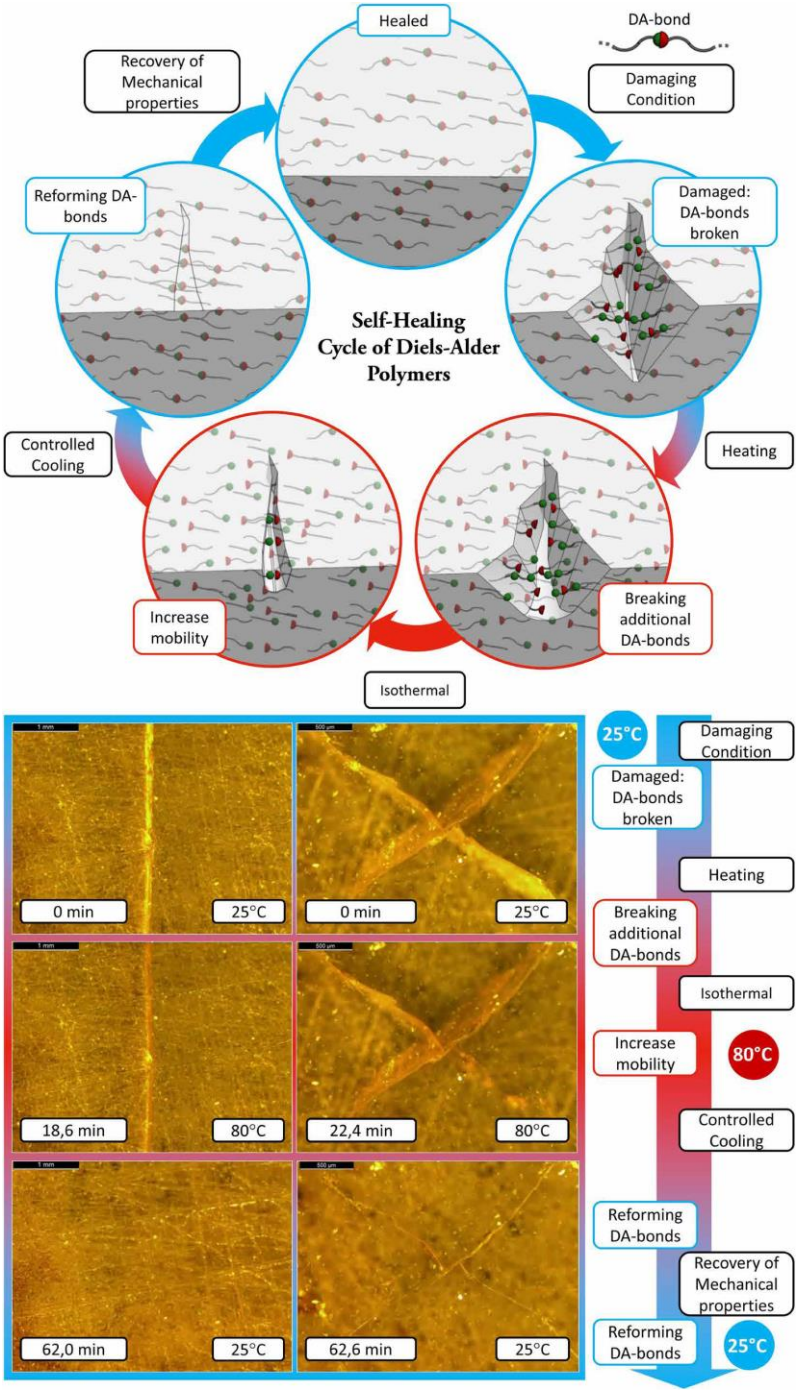

The SH procedure contains five steps: the damage, a heating step, an isothermal step, a controlled cooling, and a recovery at room temperature. The pictures illustrate the self-healing of a damaged DA polymer sample during the different stages.

2.3 Actuation and Feedback

2.3.1 Electronic Pressure Regulators

Most Soft Robot applications utilize proportional control valves to regulate pressure in the actuators. This allows precise control of the actuator. Habibian (2019) utilized a TR-025-g10s electronic pressure regulator which has the option to receive pressure feedback and control with PID within the regulator. However, hardware for such setups can be expensive in the market.

2.3.2 Fluidic Drive Cylinders

Marchese & Rus (2016) developed a high-capacity fluidic drive cylinder setup to control their soft robotic manipulator. This type of syringe-like action can provide proportional actuation similar to a pressure regulator. However, it requires specialized equipment and linear drives as in figure 2.12.

Figure 2.12

High-Capacity Fluidic Drive.

2.3.3 ON/OFF Solenoid Valves

Solenoid valves are the most common type of pneumatic control equipment available in the market. However, unlike the pressure regulators discussed above, on-off valves require two valves per actuator to perform inflation and deflation.

Booth et al. (2018) developed a Pneumatic Pressure Regulator with two on-off solenoid valves and a pressure sensor as shown in figure 2.13. This regulator operates on three states: Fill State which opens the inlet valve lets air flow into the actuator, Hold State

which holds air inside the actuator by closing both valves and Release State which opens the outlet valve to let air out. Due to the compact size of this regulator, it can be integrated as an onboard controller for mobile soft robots.

Figure 2.13

Pneumatic Pressure Regulator for Distributed Control

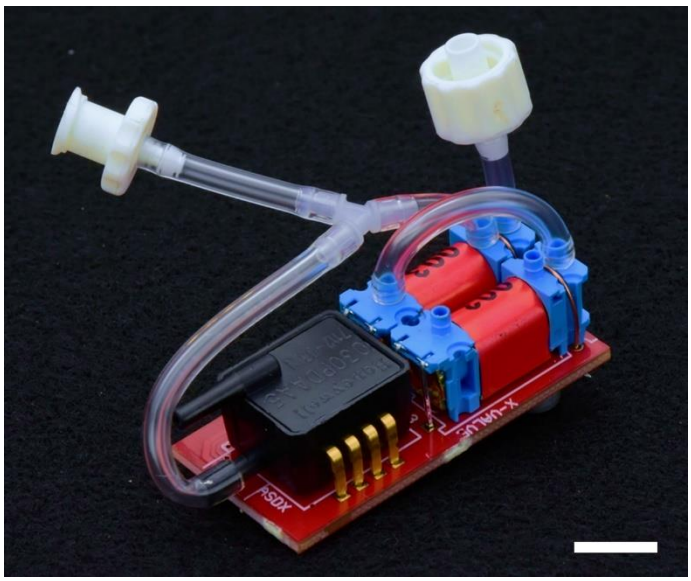

Young et al. (2019) developed PneuSoRD, which is an open-source hardware platform for soft robot control. This hardware shield which can be added to Arduino Due and can be connected to 26 on-off valves, 5 proportional valves and 12 pressure sensors. The authors also provide software support for labView, Simulink and Arduino with Bang-Bang and PID control.

2.4 Control Techniques

Control of soft robots has been a problem that is often addressed by researchers due to its complicated nature.

2.4.1 Sliding Mode Controller with PID Sliding Surface

Khan & Li (2020) proposed a Sliding Mode Controller with a PID sliding surface for active vibrations damping of pneumatic soft robots. This is mainly used to tackle the vibrations caused by rapid de-actuation of the robot. The authors mention that reduction of the vibrations will lead to reduced settling times and reduce structural defects. The authors have found that vibration damping through the SMC with PID sliding surface

for varying bending angles is far superior compared to those of regular PID controller and the SMC.

2.4.2 Robust Control

Ouyang Bo et al. (2018) develops a Robust Model-Predictive Control System for a flexible continuum robot which is used to deform soft objects. The authors established linear approximation model that maps the actuation space of the robot along with the deformation space of the object. To estimate the Jacobian matrix of the robot, a Geman-McClure (GM) estimator is designed. This estimator eliminates model uncertainty and environmental disturbances. The authors utilized a camera for visual feedback of the system.

Zheng (2020) proposes a design for a soft robot which has a similar configuration of a delta robot as shown in Figure 2.14. The robot consists of a tripod-like silicone link system actuated through three DC motors. The goal is to control the displacement of an object in the center hole of the robot. Feedback was taken through an OptiTrack vision system. After defining the linear nominal model with uncertainty, a robust controller is developed to achieve position control of the robot.

Figure 2.14

Tripod Type 3D Printed Soft Robot

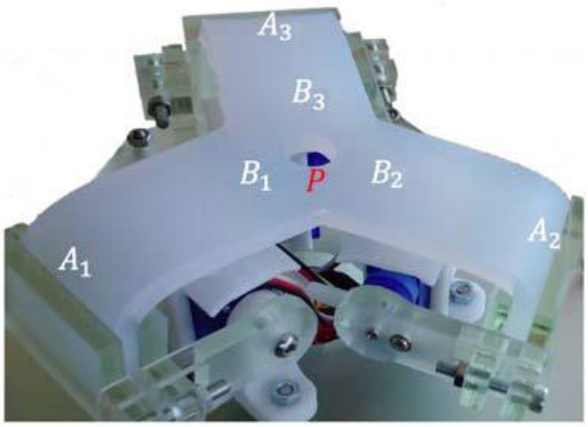

2.4.3 Reinforcement Learning Based Control

Zhang Haochong et al. (2017) proposes two concepts for soft robot control: designing the abstract representation of the state of a soft robot and developing a reinforcement learning method to derive effective control policies. The representation model is designed through piecewise model with five states/coordinates. The problem was abstracted and represented as a Markov Decision Process (MDP).

Thuruthel et al. (2019) implemented a model-based policy learning algorithm for closed loop predictive control of a soft robotic manipulator. The soft robot is a two-section manipulator with three radially symmetric pneumatic chambers.

2.4.4 Deep Learning Based Control

Truby et al. (2020) utilized a Neural Network based architecture with Long Short-Term Memory layers train the model by taking visual data as ground truth data. Thereby, the author was able to train the robot based on the inputs of a proprioceptive skin. The results of this LSTM network were compared with a shallow 2-layer Multi-Layer Perceptron (MLP) network.

Lloyd et al. (2020) developed a magnetically actuated slender silicone tentacle robot. The size of this robot makes it impossible to embed sensors in the robot body. The inverse statics of the robot is obtained through an Artificial Neural Network (ANN) trained through motor babble (repeated performance of randomized motor commands). This configuration requires a prior knowledge of the working environment such as an MRI of the brain.

CHAPTER 3
METHODOLOGY

3.1 Overview

This thesis focuses primarily on the control of the cartesian position of the robot. The robot is to be developed with 3 soft actuators. For this purpose, it is necessary to develop simulation based on the kinematic analysis of the robot to verify that the robot can achieve the objectives within the scope of the thesis. Thereby, the robot was designed and fabricated. The control system was designed based on hardware capabilities.

3.2 Kinematic Model

The robot developed in this thesis can be classified as a continuum robot as it consists of length changing actuators which result in pose changes of the manipulator. Continuum type robots utilizes its continuous sectional body to position itself unlike traditional robots which actuates distributed motors.

Thereby, it is not possible to directly map actuator space parameters to task space parameters in soft robot kinematics. Therefore, an intermediate calculation must be done in the configuration space to map the actuator space to the task space (Webster & Jones, 2010). The actuator space is dependent upon the type of robot, i.e., cable actuation, rod, tube lengths. Thereby, the mapping can be observed as in figure 3.1.

Figure 3.1

Kinematic Mapping of Continuum Robots

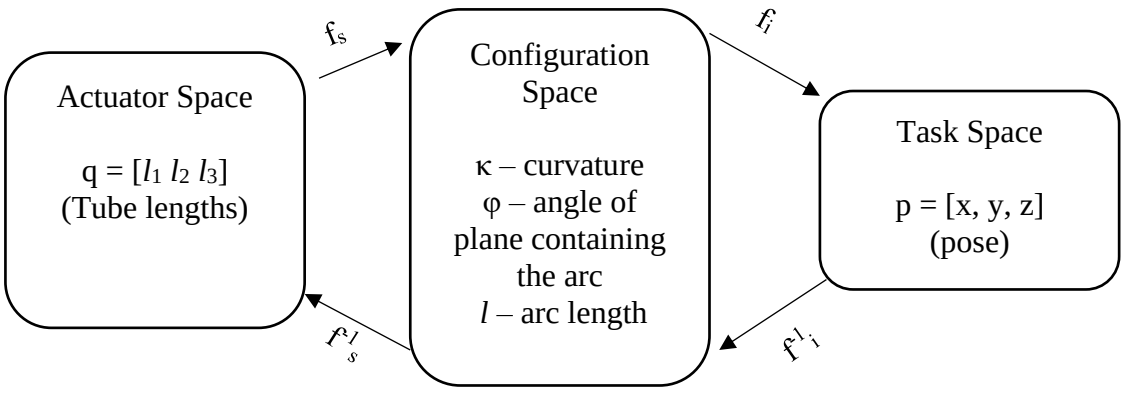

In this mapping f_s refers to the robot specific mapping which has to be derived based on the physical structure of the robot. Once the actuator space is mapped to the configuration space, the independent mapping function f_i is generally the same for any kind of continuum type robot. The independent mapping will provide position and orientation. The inverse of these mappings can be found through inverse kinematic methods.

For the derivation of the kinematics in the next two sections, the Constant Curvature assumption was taken into consideration. This assumption states that the pose of the continuum robot is not dependent on the curvature of the robot and hence remains constant throughout the length of the robot segment. Thereby, the kinematics are developed as functions of actuator length.

3.2.1 Forward Kinematics

3.2.1.1 **Robot Independent Mapping.** The forward kinematics will be initially developed with the robot independent mapping which involves the curvature, bending angle and backbone length of the robot mapped to robot pose. The backbone length refers to the length of the center of the manipulator which is the resultant of all the actuator lengths. Figure 3.2 depicts representation of the robot in the x-y-z plane.

Figure 3.2

Robot Description in X-Y-Z Plane

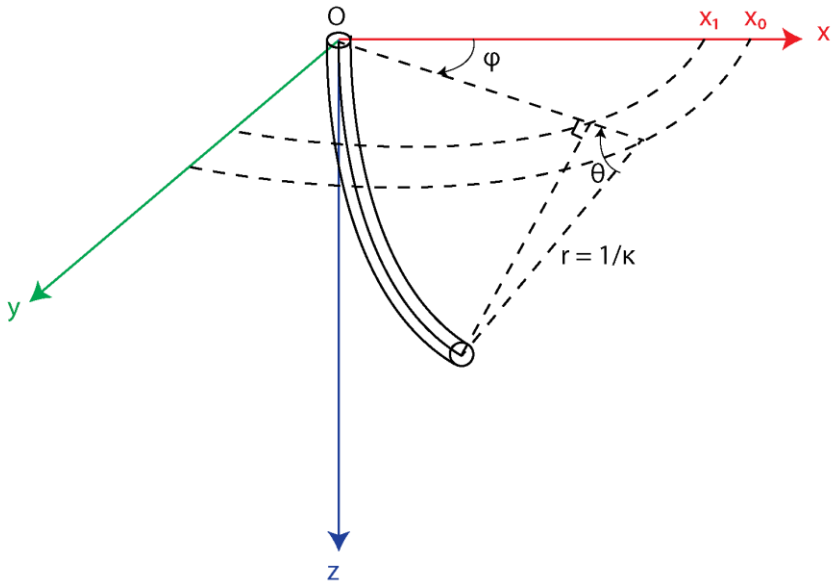

Where,

$$\phi - Angle\ of\ plane\ containing\ the\ arc$$
$$\theta - Bending\ angle\ of\ robot$$
$$r - Radius\ of\ curvature$$
$$\kappa - Curvature$$

The +Z axis is tangent to the base of the robot. For the derivation of this mapping, ϕ will be set to zero to simplify the figure 3.2 to a single plane x-z as shown in figure 3.3.

Figure 3.3

Robot in Simplified X-Z Plane

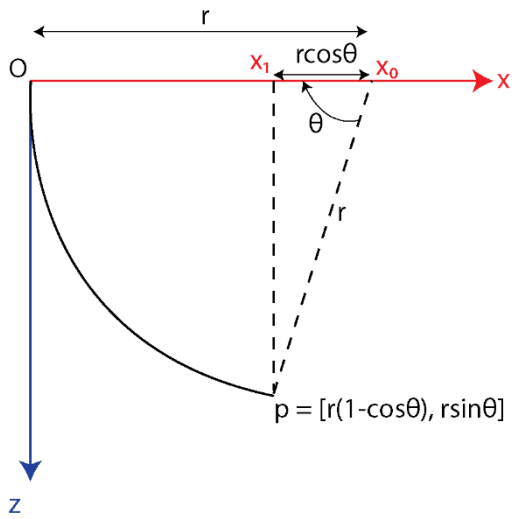

For ϕ = 0, positive curvature about +y axis traces 180° and touch the x axis. For any ϕ other than zero, the arc rotates out of the x-z plane about z axis. With reference to figure 3.3, the center of curvature rests on x axis and end effector position p can be given as,

$$p = [r(1 - \cos\theta), 0, r\sin\theta]^T \quad (1)$$

To describe the robot independent homogeneous transformation matrix, two rotation matrices will be defined as follows.

1. Motion about +y axis with θ: $R_y(\theta) \in SO_3$
2. Motion about +z axis with ϕ: $R_z(\varphi) \in SO_3$

$$T = \begin{bmatrix} R_z(\phi) & 0_{3\times1} \\ 0_{1\times3} & 1 \end{bmatrix} \begin{bmatrix} R_y(\theta) & p \\ 0_{1\times3} & 1 \end{bmatrix} \quad (2)$$

$$R_y(\theta) = \begin{bmatrix} \cos\theta & 0 & \sin\theta \\ 0 & 1 & 0 \\ -\sin\theta & 0 & \cos\theta \end{bmatrix} \tag{3}$$

$$R_z(\phi) = \begin{bmatrix} \cos\phi & -\sin\phi & 0 \\ \sin\phi & \cos\phi & 0 \\ 0 & 0 & 1 \end{bmatrix} \tag{4}$$

$$T = \begin{bmatrix} \cos\phi & -\sin\phi & 0 & 0 \\ \sin\phi & \cos\phi & 0 & 0 \\ 0 & 0 & 1 & 0 \\ 0 & 0 & 0 & 1 \end{bmatrix} \begin{bmatrix} \cos\theta & 0 & \sin\theta & r(1-\cos\theta) \\ 0 & 1 & 0 & 0 \\ -\sin\theta & 0 & \cos\theta & r\sin\theta \\ 0 & 0 & 0 & 1 \end{bmatrix} \tag{5}$$

$$T = \begin{bmatrix} \cos\phi\cos\theta & -\sin\phi & \cos\phi\sin\theta & r\cos\phi\,(1-\cos\theta) \\ \sin\phi\sin\theta & \cos\phi & \sin\phi\sin\theta & r\sin\phi\,(1-\cos\theta) \\ -\sin\theta & 0 & \cos\theta & r\sin\theta \\ 0 & 0 & 0 & 1 \end{bmatrix} \tag{6}$$

The above transformation matrix must be written in terms of arc parameters. Hence the following substitutions will be included in the final equation.

$$\kappa = \frac{1}{r} \tag{7}$$

$$\theta = \frac{s}{r} \tag{8}$$

Hence,

$$\theta = \kappa s \tag{9}$$

$$s \in [0, l]$$

Where,

$$s - any\ point\ along\ the\ arc$$

$$l -\ length\ of\ the\ arc$$

$$f_i = T = \begin{bmatrix} \cos\phi\cos\kappa s & -\sin\phi & \cos\phi\sin\kappa s & \dfrac{\cos\phi\,(1-\cos\kappa s)}{\kappa} \\ \sin\phi\sin\kappa s & \cos\phi & \sin\phi\sin\kappa s & \dfrac{\sin\phi\,(1-\cos\kappa s)}{\kappa} \\ -\sin\kappa s & 0 & \cos\kappa s & \dfrac{\sin\kappa s}{\kappa} \\ 0 & 0 & 0 & 1 \end{bmatrix} \tag{10}$$

Since the scope of this thesis focuses on controlling the robot in the translational x-y-z axes, the following equations will be considered when testing the kinematics of the robot.

$$\begin{bmatrix} x \\ y \\ z \end{bmatrix} = \begin{bmatrix} \frac{\cos\phi\,(1-\cos\kappa s)}{\kappa} \\ \frac{\sin\phi\,(1-\cos\kappa s)}{\kappa} \\ \frac{\sin\kappa s}{\kappa} \end{bmatrix} \tag{11}$$

3.2.1.2 **Robot Specific Mapping.** After obtaining the pose equations from the robot independent mapping, it is necessary to convert the arc parameters in the configuration space to the joint parameters in the actuator space. Curvature κ, angle the robot makes with x-y plane ϕ, and arc length l, will be written in terms of the tube lengths of each actuator. Thereby, the joint parameters are defined as follows.

$$q = [l_1 \quad l_2 \quad l_3]^T \tag{12}$$

Figure 3.4 and 3.5 depicts the robot representation with respect to each of its actuator lengths and arrangement between the actuators.

Figure 3.4

Robot Representation with Actuator Lengths

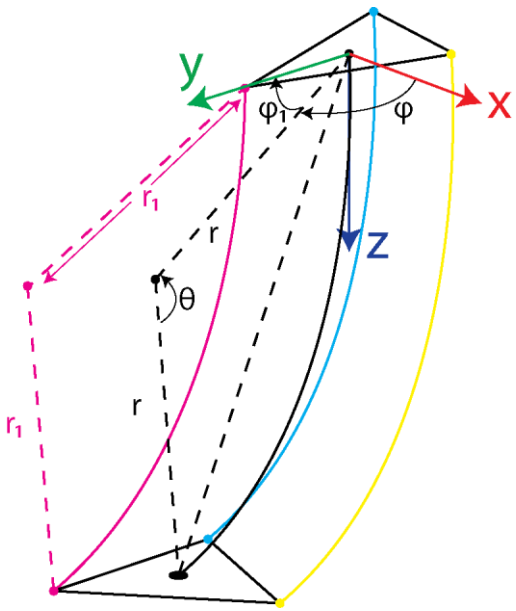

In figure 3.4, the magenta, yellow and cyan curves depict actuators 1,2 and 3 respectively, while the black curve depicts the resultant backbone curve. The other parameters are the same as defined previously. The triangle on top with x-y-z coordinate frame depicts the base of the robot while the one on the bottom with the black dot is the end effector. The black dot represents the pose of the robot. Figure 3.5 further breaks down the base geometry to assist the calculations.

Figure 3.5

Robot Base Geometry

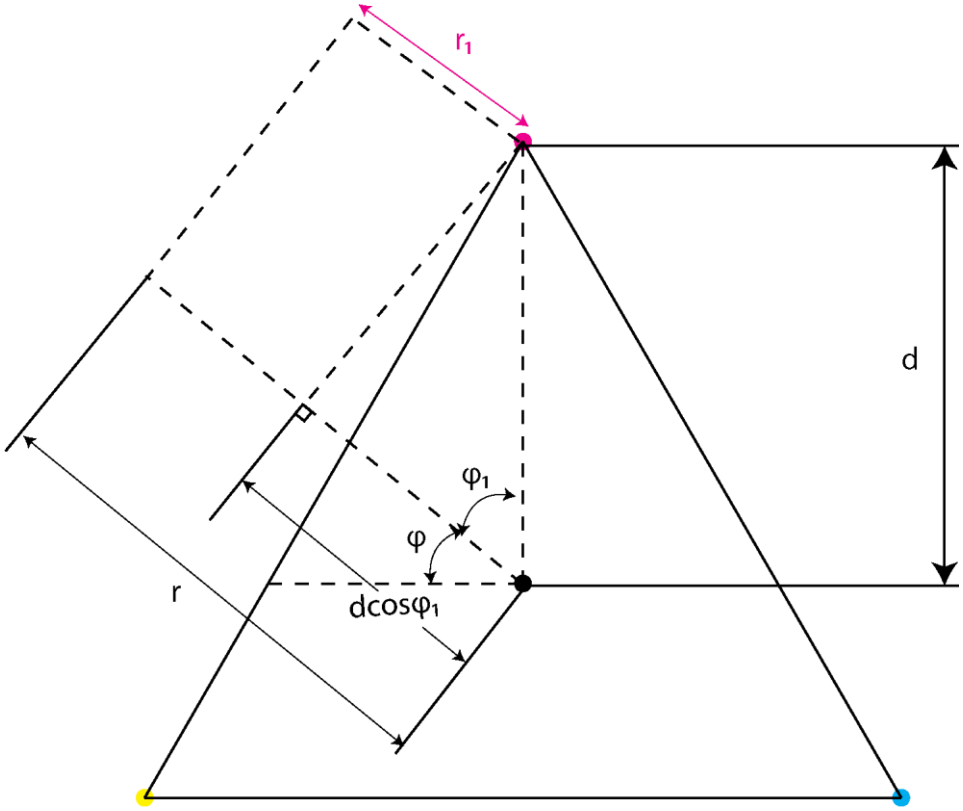

The distance between the center of the base and one actuator is denoted by d and is same for each actuator, ϕ_i ($i \in 1,2,3$) denotes the robot's bending direction with respect to each actuator. The radii r_i ($i \in 1,2,3$) refers to the radii of curvature for each of the 3 actuators. These parameters can be presented as follows.

$$r_i = r - d\cos\phi_i \tag{13}$$

Considering, the equation to compute the length of an arc,

$$l = \theta r \tag{14}$$

$$l_i = \theta r_i \tag{15}$$

Considering figure 3.4 and 3.5, the arc length of the robot *l* and arc length of ith actuator l_i can derived as,

$$l = l_i + \theta d \cos \phi_i \tag{16}$$

The bending directions can be denoted as,

$$\phi_1 = 90^o - \phi \tag{17}$$

$$\phi_2 = 210^o - \phi \tag{18}$$

$$\phi_3 = 330^o - \phi \tag{19}$$

Thereby, *l* can be written with respect to each actuator as follows,

$$l = l_1 + \theta d \cos \phi_1 \tag{20}$$

$$l = l_2 + \theta d \cos \phi_2 \tag{21}$$

$$l = l_3 + \theta d \cos \phi_3 \tag{22}$$

Combining the above 3 equations yield the arc parameter for backbone arc length *l(q)* with respect to each actuator length.

$$l(q) = \frac{l_1 + l_2 + l_3 + \theta d(\sum_{i=1}^{3} \cos \phi_i)}{3} \tag{23}$$

Through trigonometric identities, it can be shown that,

$$\sum_{i=1}^{3} \cos \phi_i = 0 \tag{24}$$

This provides the arc length equation as,

$$l(q) = \frac{l_1 + l_2 + l_3}{3} \tag{25}$$

From the 3 variants of *l* mentioned above, the following relationships can be derived,

$$\theta d = (l_2 - l_1)/(\cos \phi_1 - \cos \phi_1) \tag{26}$$

$$\theta d = (l_3 - l_2)/(\cos \phi_2 - \cos \phi_3) \tag{27}$$

Thus, equating the above two relationships and simplifying, it is possible to obtain the bending direction angle $\phi(q)$ as follows,

$$\phi(q) = \tan^{-1}\left(\frac{\sqrt{3}(l_2 + l_3 - 2l_1)}{3(l_2 - l_3)}\right) \tag{28}$$

For the curvature function of the robot, it is recalled from equations 7, 8 and 9,

$$\theta = \kappa l = {}^{l_i}/_{r_i} \tag{29}$$

Which gives,

$$r_i = {}^{l_i}/_{\kappa l} \tag{30}$$

Using the relationship in equation 11, the following equation is obtained,

$$\kappa = \frac{(l - l_i)}{ld\cos\phi_i} \tag{31}$$

By substituting i = 1,

$$\kappa = \frac{(l_2 + l_3 - 2l_1)}{(l_1 + l_2 + l_3)d\sin\phi} \tag{32}$$

Using the following trigonometric identity,

$$\sin\left(\tan^{-1}\left({}^{y}/_{x}\right)\right) = {}^{y}\Big/\sqrt{x^2 + y^2} \tag{33}$$

The curvature function can be derived as follows,

$$\kappa(q) = \frac{2\sqrt{l_1^2 + l_2^2 + l_3^2 - l_1l_2 - l_1l_3 - l_2l_3}}{d(l_1 + l_2 + l_3)} \tag{34}$$

Finally, the mapping for the configuration space parameters to actuator space parameters can be given by equation 23, 26, and 32.

3.2.2 Inverse Kinematics

With the inverse kinematics, it is possible to derive the tube lengths for each actuator with respect to x-y-z position at any given pose. Similar to the mappings of the forward kinematics, firstly the task space will be mapped to the configuration space to get

bending direction angle, curvature and bending angle. Thereby, those parameters can be mapped to obtain tube lengths (Meng et al., 2013).

Referring to figure 3.2 in the previous section, the following derivations can be made,

$$\phi = \tan^{-1}\left(\frac{y}{x}\right) \tag{35}$$

$$x_1 = \sqrt{x^2 + y^2} \tag{36}$$

From figure 3.3, applying Pythagoras theorem to Δpx_1x_0 the following relationship can be obtained,

$$r^2 = (r - x_1)^2 + z^2 \tag{37}$$

Substituting x_1 from equation 36 to equation 37 and considering equation 7,

$$\kappa = \frac{2\sqrt{x^2 + y^2}}{x^2 + y^2 + z^2} \tag{38}$$

Considering cosine law in Δpx_1x_0, for $z > 0$,

$$\theta = \cos^{-1}\left(\frac{r - x_1}{r}\right) \tag{39}$$

For $z < 0$,

$$\theta = 2\pi - \cos^{-1}\left(\frac{r - x_1}{r}\right) \tag{40}$$

Substituting for x_1 from equation 36 and r from equation 7,

$$\theta = \begin{cases} \cos^{-1}(1 - \kappa\sqrt{x^2 + y^2}) , & z > 0 \\ 2\pi - \cos^{-1}\left(1 - \kappa\sqrt{x^2 + y^2}\right) , & z \leq 0 \end{cases} \tag{41}$$

Finally, considering the equations 16 and 29, the angle ϕ_i can be replaced such that the actuator lengths can be calculated as follows,

$$l_i = \frac{\theta}{\kappa} - \theta d \cos\left(\frac{2\pi}{3}(i - 1) + \frac{\pi}{2} - \phi\right) \tag{42}$$

3.3 Simulation

The simulation for the kinematic analysis was done in MATLAB 2020a. Firstly, the forward kinematics was tested based on the changing of the robot actuator lengths. Thereafter, inverse kinematics was developed and compared against the forward kinematics for verification. For the physical parameters of the robot, certain values were used with respect to the available hardware components and physical design of the robot.

3.3.1 Forward Kinematics Simulation

Initially, a MATLAB function was derived to input the length values and output the x-y-z position values. In order to draw the robot, the formulae of the forward kinematics were used to draw the backbone arc. The arc was plotted with a predetermined resolution where the forward kinematic function is used for each resolution point.

Thereafter, a live script was created to manually change input to visualize how the robot behaves with the change of actuator lengths. Figure 3.6 depicts the live script in operation with different robot positions. Due to the physical constraints of the hardware setup, the length of actuators based on pressure presets will be compared against its simulation counterparts.

Figure 3.6

Forward Kinematics Simulation

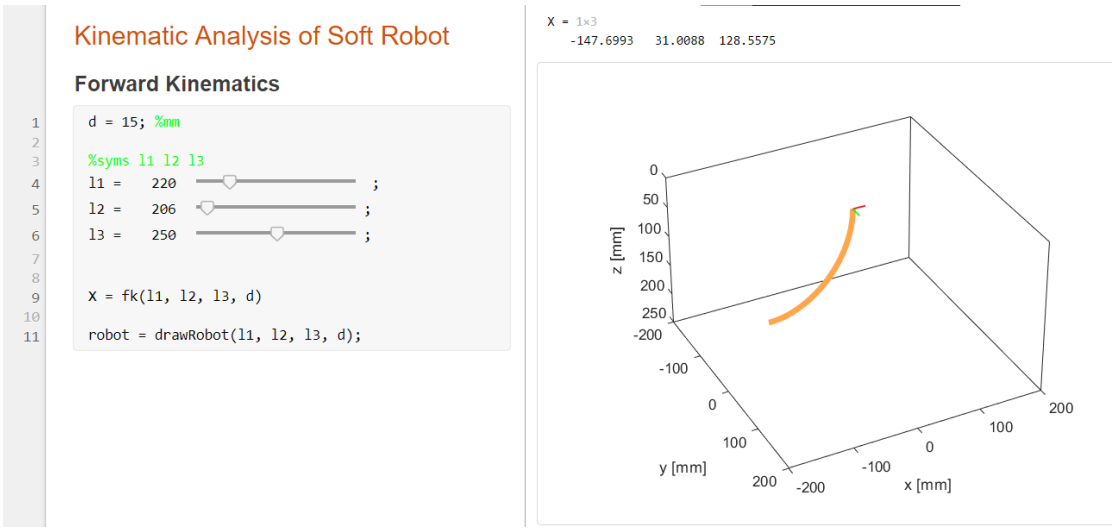

In figure 3.6, d refers to the distance between the center of the base and one actuator which is the same parameter described in the previous subsection. The d value is set to 15mm as it is constrained in the hardware model due to the material and components used. The lengths defined as l_1, l_2 and l_3 are the actuator lengths which acts as inputs to the forward kinematics function “fk()”. X is the output of the “fk()” function and provides a 1x3 array which includes x, y, and z values. The “drawRobot()” function too accepts length values and outputs a 3D figure depicting the backbone curve of the robot in orange as observed in the right side of figure 3.6.

3.3.2 Inverse Kinematics Simulation

The function for inverse kinematics “ik()” accepts the x, y, and z values as inputs and utilizes the equations developed in the subsection 3.2 to obtain the necessary actuator length values. Figure 3.7 depicts the live script of the inverse kinematics simulation. To verify whether the results of inverse kinematics is valid, the forward kinematics function “fk()” was called and it can be observed that the values are identical. Finally the “drawRobot()” function was used to graphically view the robot pose as before.

Figure 3.7

Inverse Kinematics Simulation

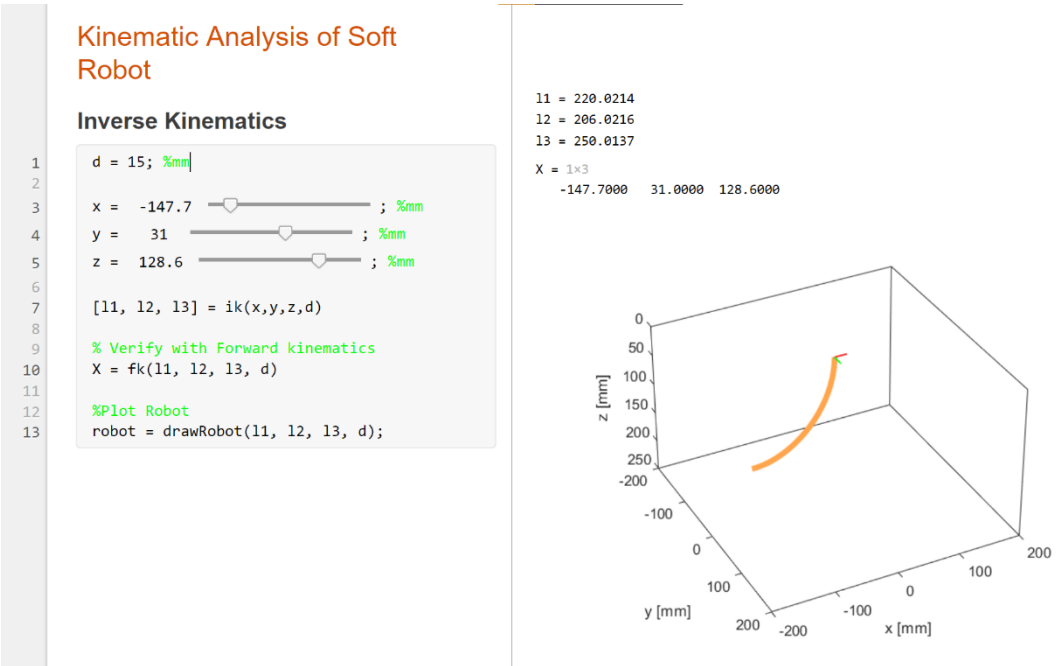

As can be expected, the inverse kinematics yield coherent results in comparison with the forward kinematics. Furthermore, the 3D plot of both figures 3.6 and 3.7 depict the

same robot pose. The simulation results will be compared against the hardware setup in the next chapter. For that purpose, the pressure presets suitable for the hardware setup will be used.

3.4 SOLIDWORKS Design

The mechanical design was developed through SOLIDWORKS 2020. The main robot assembly consists of the manipulator, gripper, and the frame.

3.4.1 Manipulator

The manipulator consists of three actuators. The ideal type of flexible actuator for a delta robot would be a bellow type actuator. However, the fabrication process requires much effort and require special materials and processes to develop the bellows. Hawkes et al. (2016) proves that the RPAM showcases near linear behaviour in terms of input pressure and length output. Thereby, considering the convenience of fabrication along with the advantage of near linearity, it was decided that the Reverse Pneumatic Artificial Muscle (RPAM) was suitable for this thesis.

The design for the RPAM was decided upon the physical parameters of the available material that will be further discussed in subsection 3.5. Figure 3.8 depicts the SOLIDWORKS design of the actuator that was developed. The actuator consists of a rubber tube of 16mm internal diameter and 200mm length along with the reinforcement fiber. Figure 3.9 depicts the operation of the designed actuator.

Figure 3.8

Actuator Design

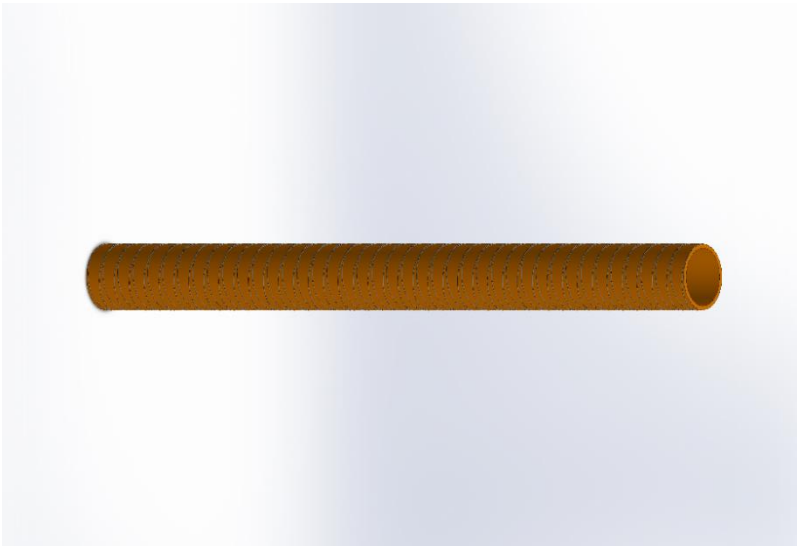

Figure 3.9

Actuator Operation Principle

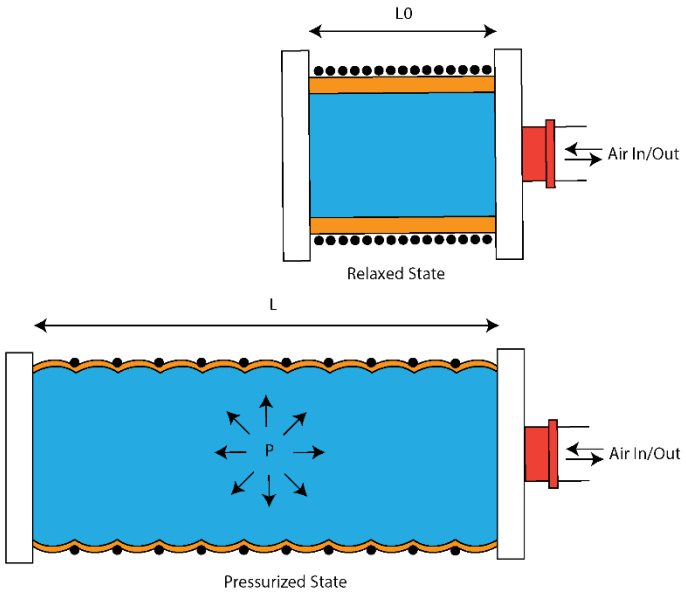

Hawkes et al. (2016) mentions that higher number of wrappings, lower operating pressures and thicker tube walls reduces the radial expansion of the rubber tube i.e., ballooning. However, it is difficult to densely wrap the actuator with a small space between the wrappings due to the manual fabrication process. Furthermore, using thicker walls require higher pressure force to actuate. Thereby, several tradeoffs had to be made with respect to the available equipment and materials.

In order to negate the effects of twist in the helical direction, the fiber reinforcement was designed as a double helix pattern with a pitch of 5mm. This ensures the length of the tube has 40 fiber windings per helix.

The manipulator consists of a fixed base and a free moving end effector. Early iterations of the above-mentioned fixtures were designed to be single parts. However, it was noted that the sealing and repairability is greatly hindered by such a design. Thereby, each actuator was designed with isolated end caps which can be fitted to the base/end effector plate with ease. Figure 3.10 depicts the end caps for the actuators, figure 3.11 depicts the base and end effector plates while figure 3.12 depicts the assembly of the base and effector. The top endcap has a hexagonal cutout to include a threaded insert that will support a pneumatic fitting. The bottom endcap is completely sealed.

Figure 3.10

Endcaps a) Top Endcap b) Bottom Endcap

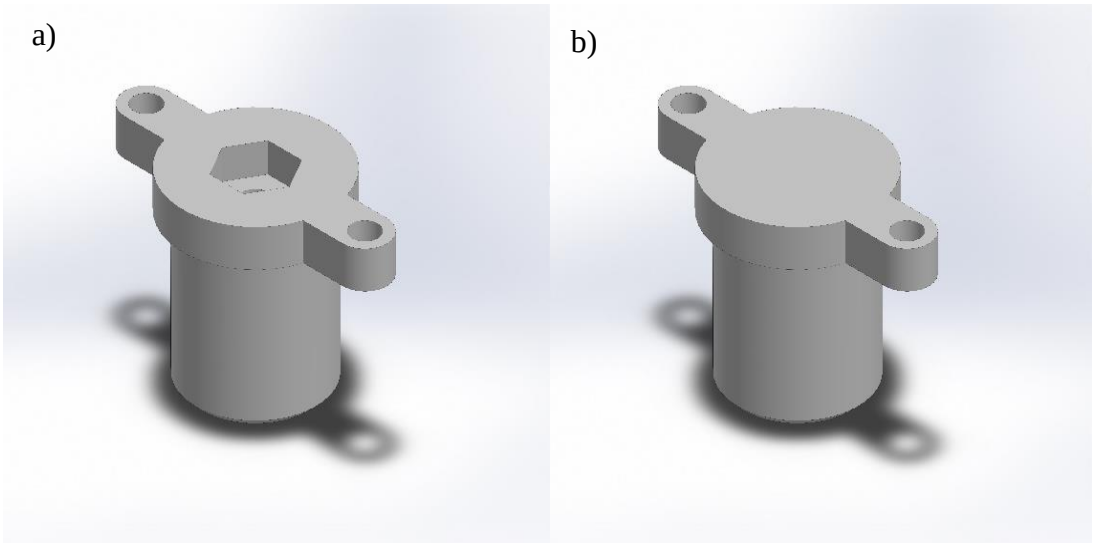

Figure 3.11

End Plates a) Base plate b) End Effector plate

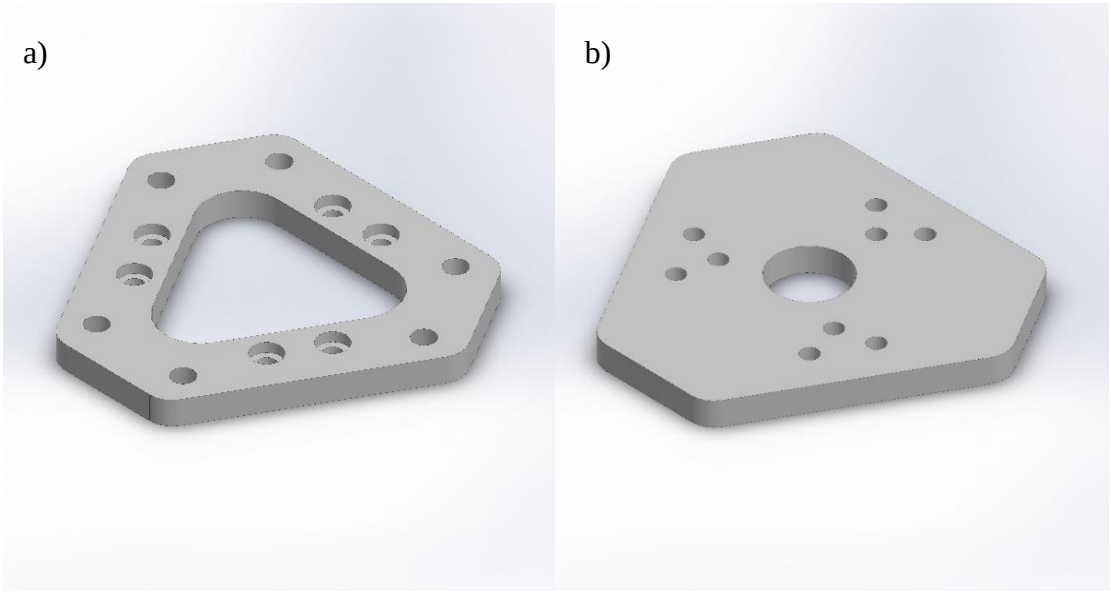

Figure 3.12

End Plate Assembly a) Base b) End Effector

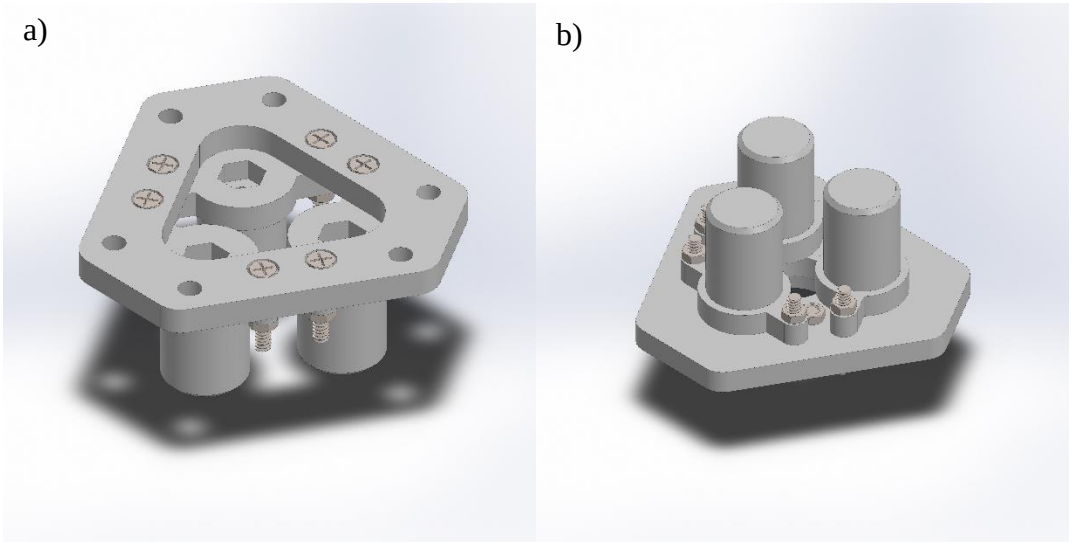

Finally, the three RPAM actuators were assembled with the base and end effector plates together with hose clamps and the pneumatic fitting as shown in figure 3.13.

Figure 3.13

Manipulator

3.4.2 Gripper

Since the main focus of this thesis is the manipulator, the gripper design is a generic design suitable to hold a SG90 micro servo motor from the open-source 3D model library GRABCAD (Thierry Soriano, 2019). Figure 3.14 depicts the design of the gripper that will be utilized for this thesis.

Figure 3.14

Gripper Mechanism

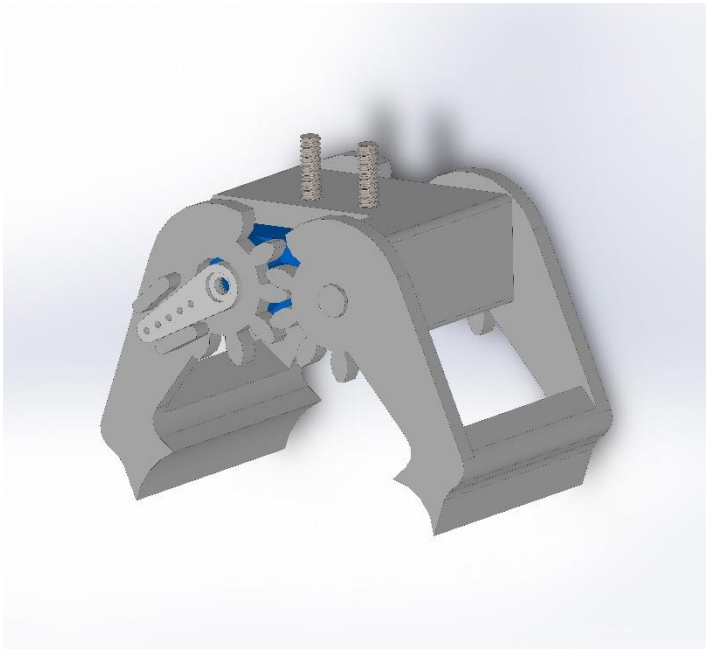

3.4.3 Frame

In order to hold the manipulator and test its positioning capabilities, a 30cmx30cmx30cm aluminium profile frame was designed. The frame was topped with an acrylic plate which provides space for electrical and pneumatic routing of the robot. Figure 3.15 depicts the frame design.

3.4.4 Final Robot Assembly

Figure 3.16 depicts the full assembly of the robot. As per the kinematic derivation, the z axis is pointing downwards. However, due to the usage of aluminium profiles, it is possible to change the z axis orientation depending on the requirement.

Figure 3.15

Frame

Figure 3.16

Full Assembly of the Robot

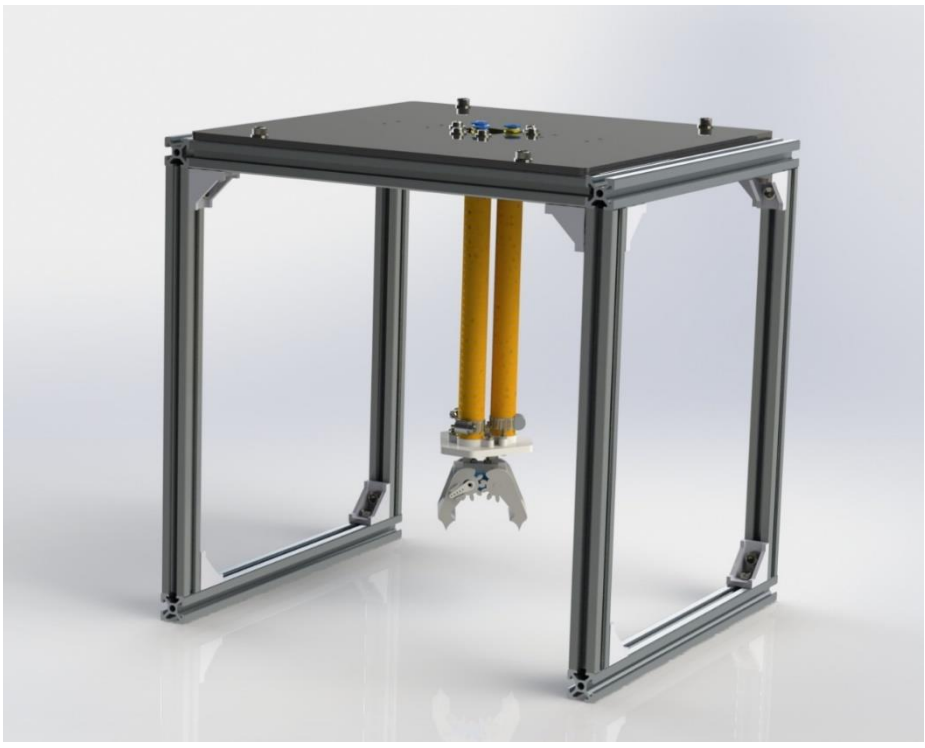

3.5 Fabrication

3.5.1 3D Prints

The base, end effector and gripper parts were 3D printed with PLA plastic as it is a convenient way of fabricating more detailed parts. For the case of the base and the end effector, several updates had to be made to obtain the most effective design. Rather than using the design shown in figure 3.17, isolating each actuator on the base and effector makes it more modular and provides better support for future design updates.

Figure 3.17

Early Version of End Effector and Base

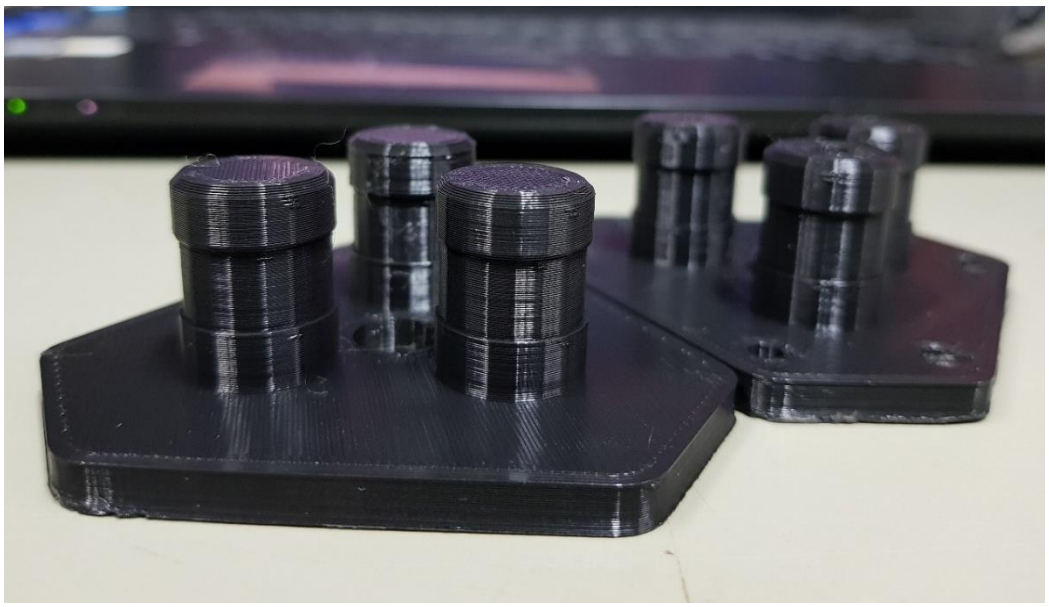

Another issue from the above design that arose was the leakage of air through the gaps in the 3D print. Although solid, the print is done layer by layer which allows for minute gaps within the layers which causes air leakage during actuation. The solution for this is to seal the prints with epoxy resin. Application of the epoxy is cumbersome in the above design; therefore, the final update allows convenient application of epoxy for the end caps as shown by the glossy texture of the 3D prints in figure 3.18.

It can also be noted in figure 3.18 that the three end caps on the right contain an M5 nut fitted on the hexagonal slot as per the design in figure 3.10(a). This allows the usage of a M5 threaded 6mm cannula pneumatic fitting as shown in figure 3.19. Such a fitting will provide extra protection against air leakages as it contains an O-ring which will fit

tightly when screwed. The M5 nuts were inserted by using a soldering iron which partially melts the surrounding material and pushes the nut up to the end of the slot. As the PLA cools, the nut will be securely fitted on the end cap with no possibility of leakage.

Figure 3.18

Actuator End Caps

Figure 3.19

Pneumatic Fitting

(https://www.lazada.co.th/products/i571140981-s1048580474.html)

Thereafter the end caps can be assembled to the base and end effector plates as shown in figure 3.20. The gripper parts were obtained from the open-source library as mentioned in subsection 3.4, hence, the CAD files were directly 3D printed. Thereafter,

the SG90 servo motor was attached to the gripper mechanism along with the 3D printed gripper connector to attach to the end effector as shown in figure 3.21.

Figure 3.20

Robot Base and End Effector

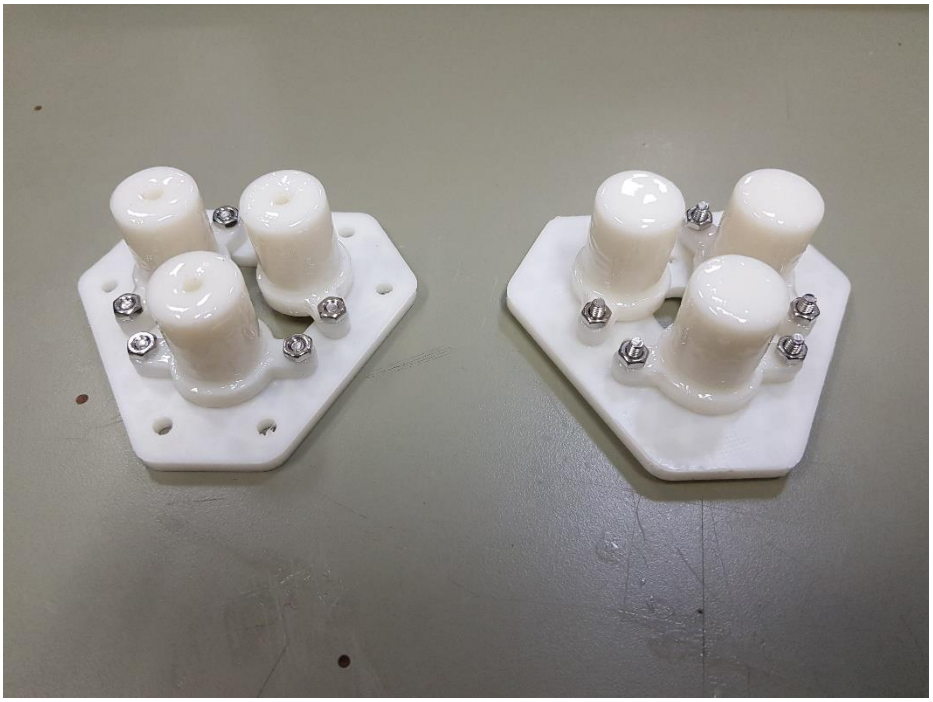

Figure 3.21

Gripper Mechanism

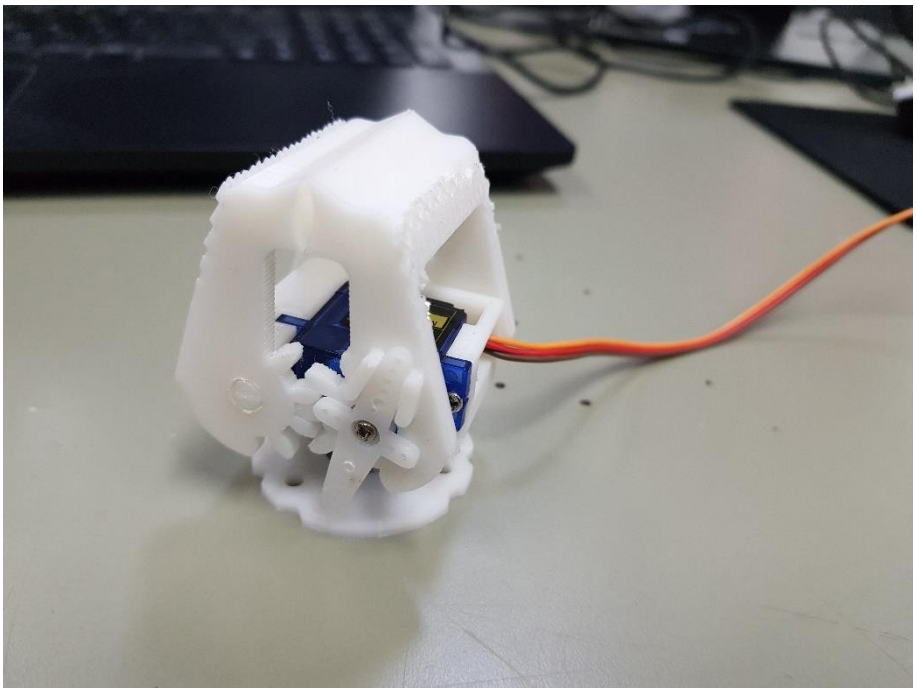

3.5.2 Actuator Fabrication

The fabrication of the actuator required several iterations of trial and error. The proper materials required were obtained from various literature sources and similar products available were utilized for this thesis. The following list contains the key ingredients utilized to fabricate the actuator and figure 3.22 depicts the materials used.

1. Latex Rubber Tube (16mm internal diameter, 1.05mm wall thickness)
2. Nylon Fishing Line (0.205mm thickness)
3. Rubber cement
4. Natural Latex Rubber Liquid

Figure 3.22

Actuator Materials a) Latex Tube b) Fiber c) Rubber Cement d) Liquid Latex

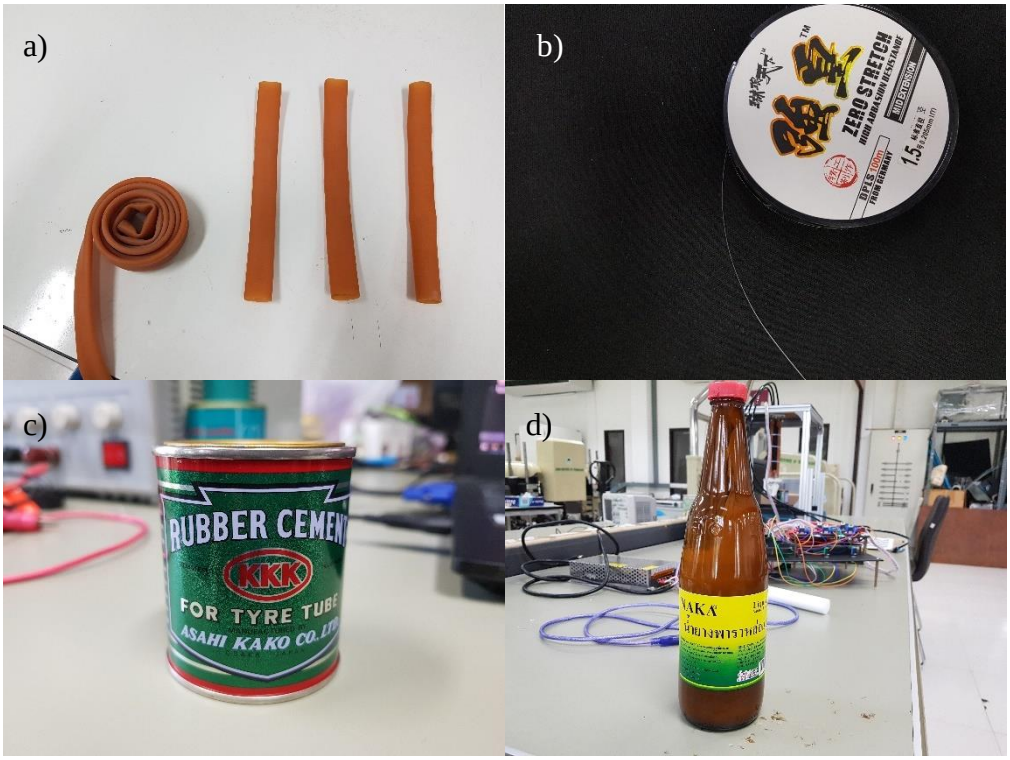

Figure 3.23 depicts the flowchart indicating the fabrication process. The process begins with cutting the tube with at least 210mm length. Thereafter, a 3D printed mold guide was inserted into the tube piece by piece. Figure 3.24 depicts the exploded view of the mold design along with the 3D printed parts. This mold was designed as 6 parts to ease the release process once the actuator is fabricated. If designed as one solid guide mold, the fiber constricts the tube, and the removal will damage the actuator. The mold was

designed such that the far ends stick out and can be easily fit onto a makeshift aluminium profile jig as utilized throughout the fabrication process.

Figure 3.23

Actuator Fabrication Flowchart

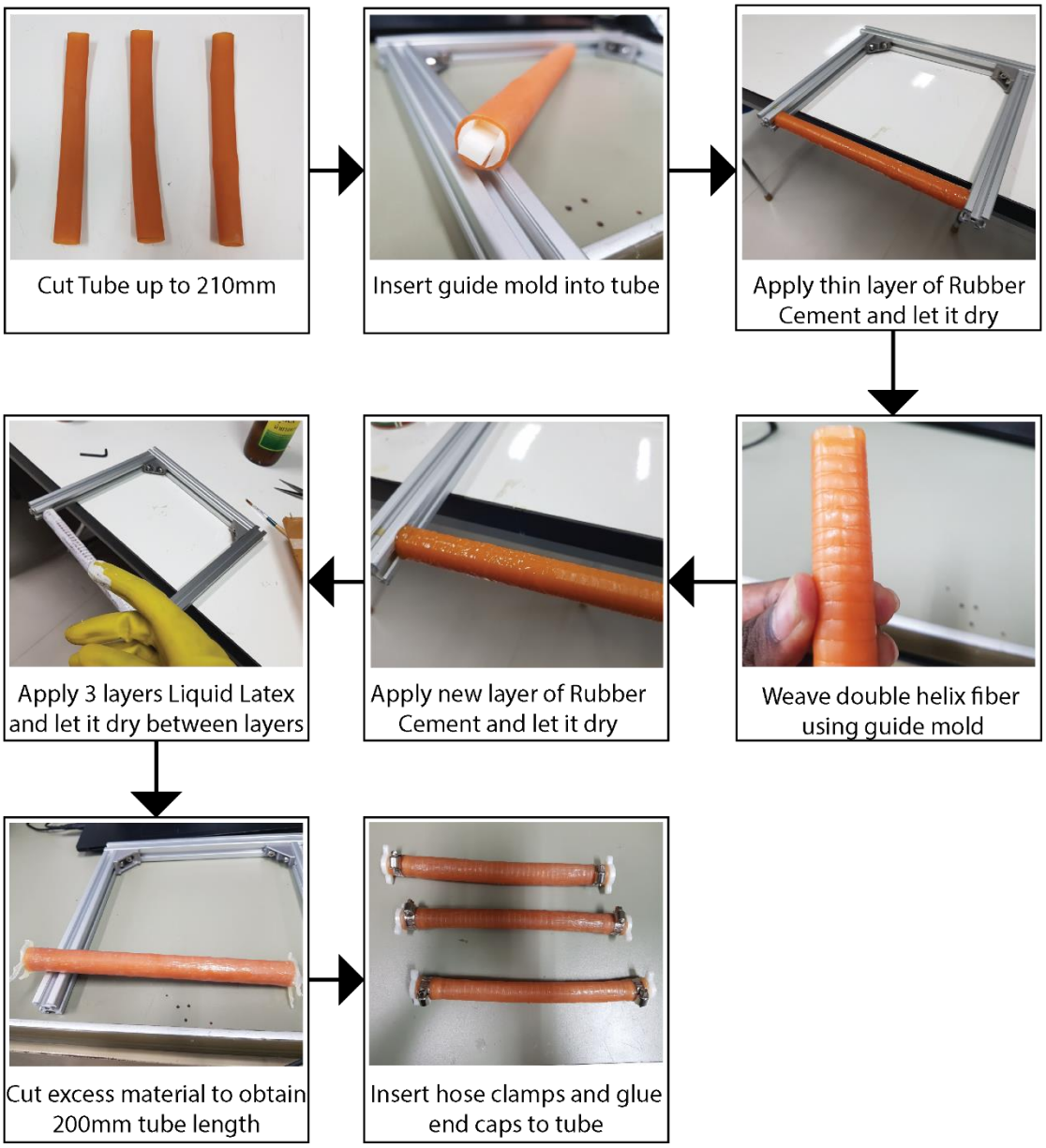

Next, the tube was secured on the makeshift jig fixture and a thin layer of rubber cement was applied using a paint brush. Once the rubber cement dried, the tube became adhesive, and the fiber could be held in place. Thereafter, the tube was removed from the jig and the fiber was weaved around as per the guide mold 5mm spacings both clockwise and counterclockwise. Subsequently, another layer of rubber cement was applied to ensure that the fiber is finely stuck on the tube.

Figure 3.24

Actuator Guide Mold a) Design b) 3D print

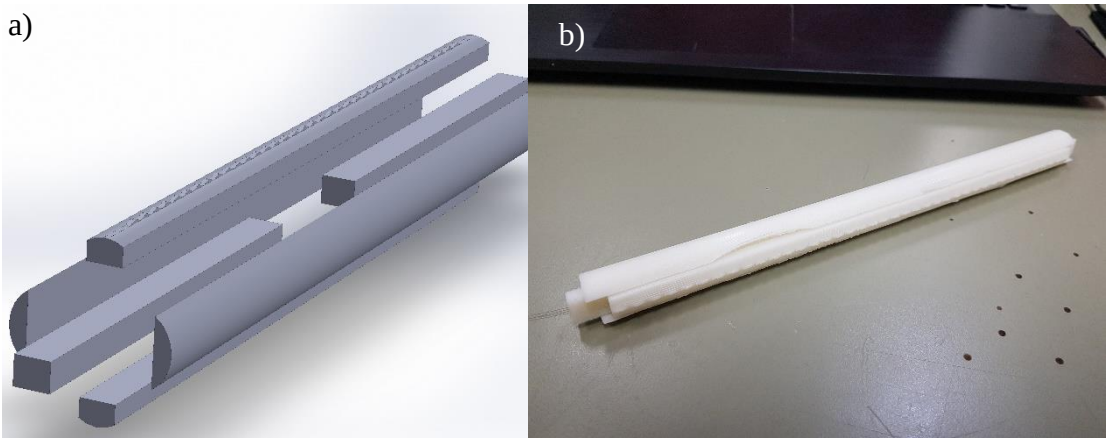

Once the rubber cement has dried, the liquid latex was applied on to the tube. The liquid latex is much less viscous compared to Elmer's glue. However, it is difficult to apply the liquid latex with a brush as it leaves brush marks and striations. Thereby, a smooth gloved finger as shown in figure 3.23 is more suitable to apply a thick layer of latex. While still on the fixture, the tube was allowed to dry before applying the next two layers. It is necessary to flip the fixture over to avoid the liquid latex collecting on the bottom side of the tube.

The actuator is ready to be taken out of the fixture after the 3rd layer has dried. The amount can be increased if necessary. For this thesis, the 3 layers of latex was adequate for the actuator to operate without much wear and tear. Additional layers may cause the actuator to be thicker than necessary. Finally, excess material was cut off and actuator was adjusted to a length of 20cm. Thereby, epoxy glue was applied to the end caps and the actuators were pushed on to the end caps. When the glue solidifies, the actuators will be thoroughly sealed. Hose clamps were utilized to ensure that the tubes are tightly sealed around the end caps.

Table 3.1 provides the specifications of the actuator developed. Although each actuator may have slight variations between them due to the manual fabrication process, all 3 actuators roughly possess the specifications provided in table 3.1.

Table 3.1

Actuator specifications

Actuator Specification	Value
Weight with latex coatings	18g
Length	20cm
Thickness of tube with latex	2.5mm
Number fiber turns per helix	40
Space between turns (pitch)	5mm

3.5.3 Manipulator Assembly

Figure 3.25 depicts the assembled manipulator. However, pressurizing a single actuator will cause the actuator to buckle as the other actuators remain the same length. Thereby, 15cm pieces of foam were inserted between the actuators to provide more support and cable ties were used to hold all the components together during actuation as in figure 3.26.

Figure 3.25

Assembled Manipulator

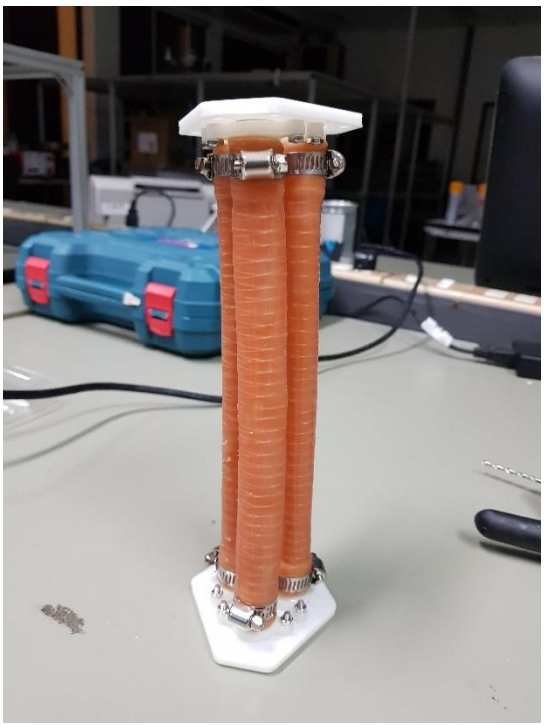

Figure 3.26

Manipulator with Foam Support and Cable Ties

3.5.4 Frame Assembly

The frame was assembled with 20x20mm aluminium profiles. Initially the frame was constructed to be of dimension 30cmx30cmx30cm. However, additional height was added by fixing more aluminium profiles to the frame legs. The top was covered with a Perspex sheet where the robot base can be bolted on. This configuration allows the robot to be fixed with either the z axis pointing upward or downward. Furthermore, the pneumatic tubing along with electronic wiring can be easily routed out of the working environment. Figure 3.27 depicts the frame assembly of the robot.

Figure 3.27

Robot with Frame Assembly

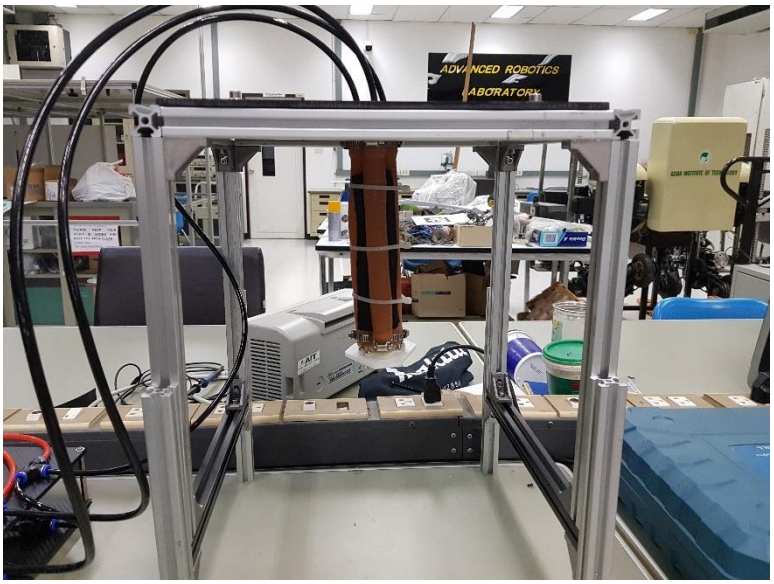

3.6 Hardware

3.6.1 Pneumatic Circuit

Throughout the various literature sources reviewed, the authors have used different methods to control fluid pressure and flow of the soft actuators as discussed in section 2.3. Components such as electronic pressure regulators may be far too costly and low-cost fluidic drive cylinders may not have enough capacity to pressurize the actuator.

A miniature DC air pump was tested as a pressure source. Although it is convenient to integrate to the setup, the DC pump cannot provide adequate pressure and will stall at certain pressures. Thereby, it is necessary to utilize a silent air compressor as shown in figure 3.28. This type of compressor will continuously provide airflow to the robot.

Figure 3.28

Silent Air Compressor

With the resources and budget available, it was decided to utilize solenoid valves to control pressure inside the actuator. Thereby, two 2/2 way solenoid valves were utilized per actuator to in order to control the pressure. One valve will allow airflow into the actuator for inflation while the other acts as an exhaust valve. Further explanations of pressure control will be included in section 3.7. The valves utilized is presented in figure 3.29.

Figure 3.29

2/2 way Solenoid Valve

Several key safety adjustments were made since safety is of paramount importance with respect to the development of soft robots. As the compressor releases air at a high flow rate, the actuator will be pressurized very fast. Thereby, there may be a chance that the control system is not fast enough to de-actuate the robot and that would result in actuator burst. Therefore, it was decided that the air supply is throttled using a speed controller valve with minimum airflow allowed. Even though the response is slower, the robot control can safely actuate the robot. Furthermore, exhaust valve too was throttled to minimize the de-actuation vibrations.

Although the actuator can robustly extend its length. At gauge pressures above 150kPa the latex coating on the actuator starts to break down such that the fiber rolls around and cause an irregular ballooning effect as shown in figure 3.30. Thereby, the maximum gauge pressure in the actuator is limited to 125kPa.

Figure 3.32 depicts the schematic of the pneumatic circuit of the robot developed in Festo FluidSim Pneumatics. A spring return single acting cylinder represents a Soft Actuator as it basically operates with the same principles. Figure 3.31 depicts the pneumatic hardware implementation of the circuit.

Figure 3.30

Actuator Bursting

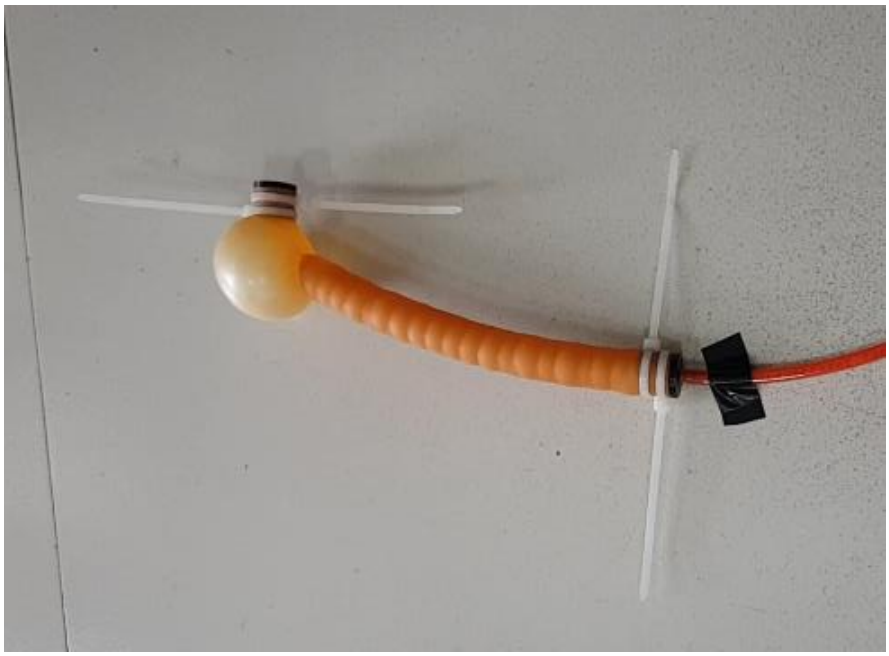

Figure 3.31

Pneumatic Circuit Hardware Implementation

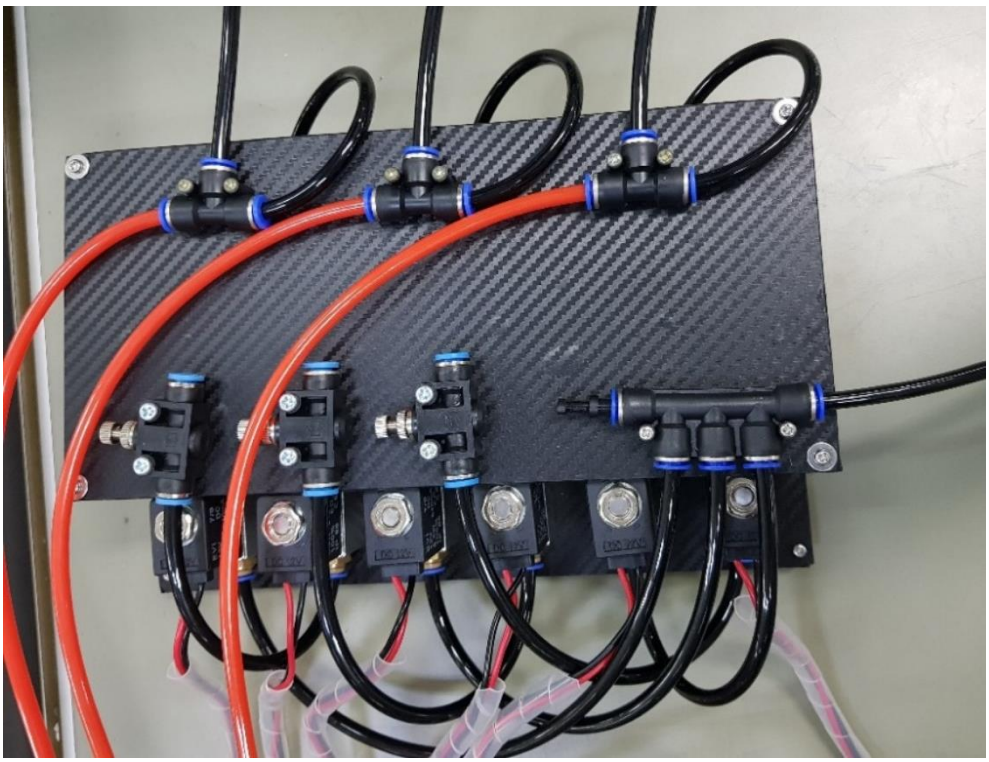

Figure 3.32

Pneumatic Circuit Schematic

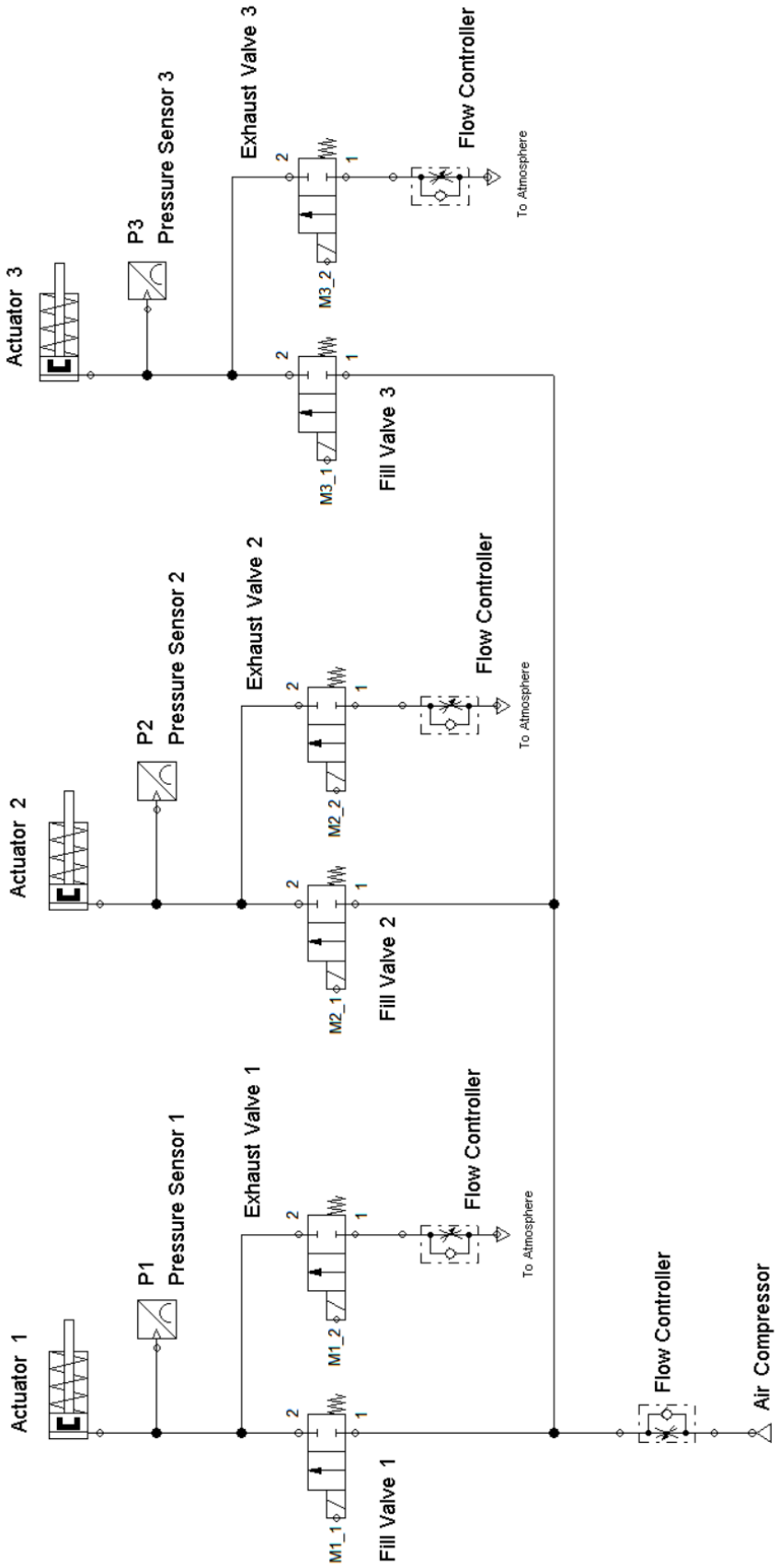

3.6.2 Electronic Circuit

The electronics utilized for this thesis are the microcontroller, pressure sensors, potentiometers, MOSFET drivers, solenoid valves, SG90 micro servo motor and power supply. Arduino MEGA was used as the microcontroller.

Three MPX5700DP differential pressure sensors were used to obtain pressure feedback. Figure 3.33 depicts the pressure sensor along with its schematic diagram. The pressure sensor contains two 4mm ports where one port was connected to the actuator and the other end was left open. This provides a differential pressure between the actuator and the atmosphere, essentially providing the gauge pressure of the actuator. The pressure sensor is capable of reading pressures up to 700kPa. Sensor noise was suppressed in the software by using a Low Pass filter.

Figure 3.33

MPX5700DP Pressure Sensor a) Sensor b) Schematic

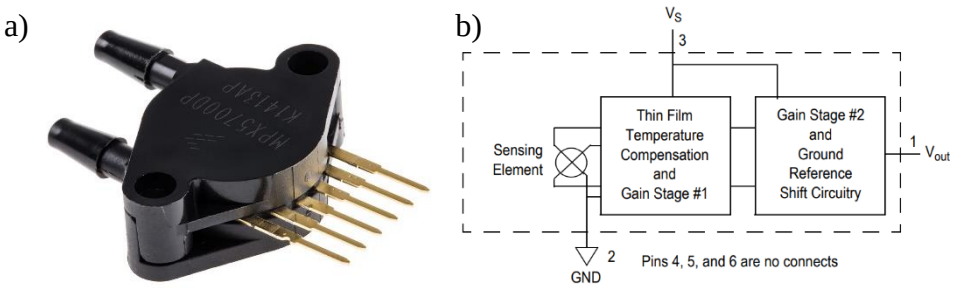

Three standard 10kΩ potentiometers were used to manually provide the three pressure setpoints. Six valves were utilized as pairs for each actuator. The valves were referenced in figure 3.29. To actuate the solenoid valves, six IRF520N MOSFET drivers as shown in figure 3.34 were used per valve. The control signal is sent from the microcontroller to the driver and the driver is powered by a 12V Switch Mode Power Supply (SMPS).

Figure 3.34

IRF520N MOSFET Driver

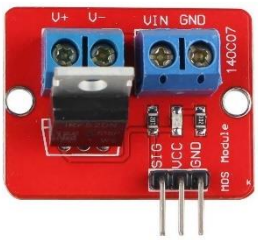

Figure 3.35

Breadboard View of Electronic Circuit

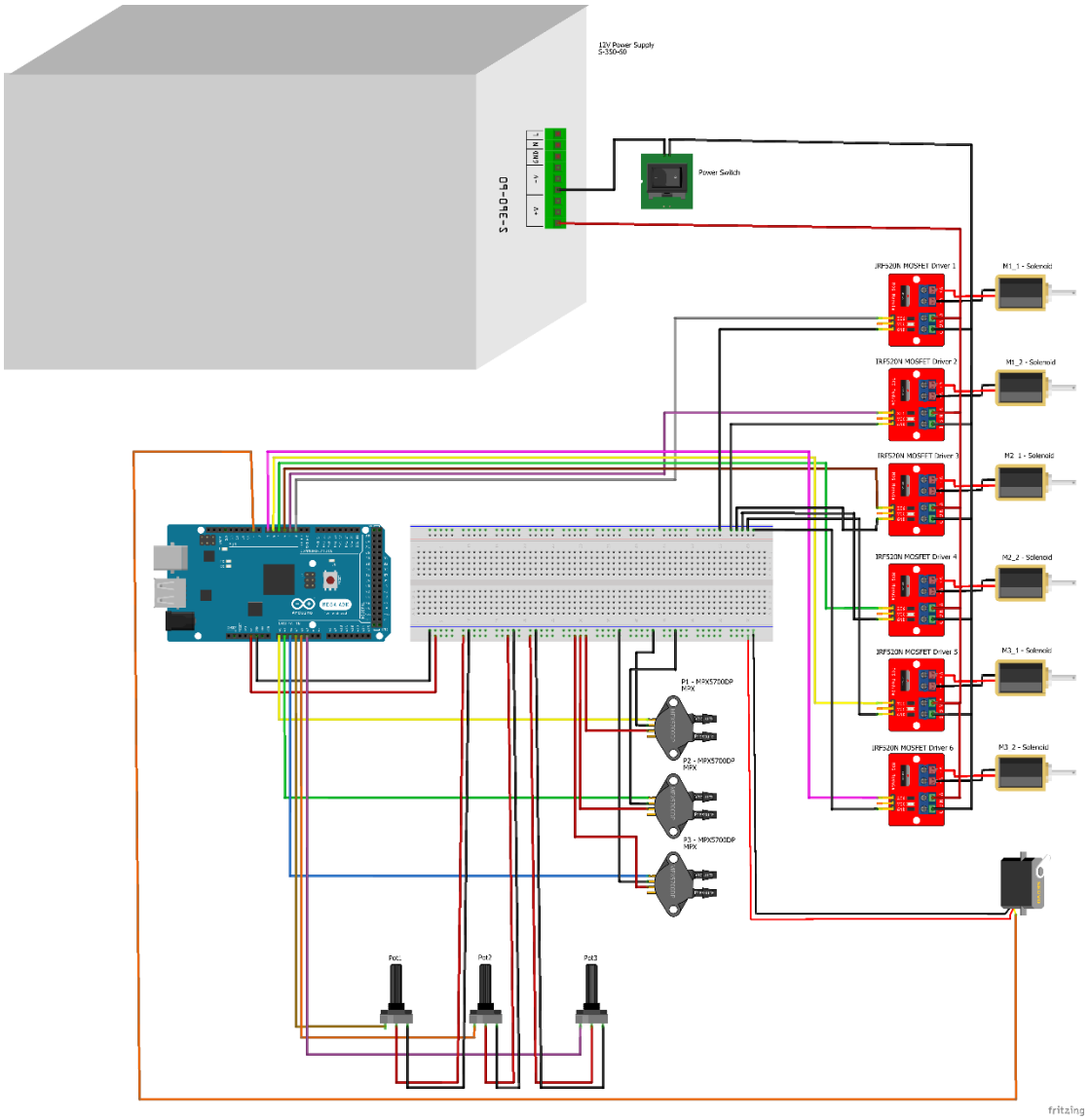

Figure 3.36

Schematic view of Electronic Circuit

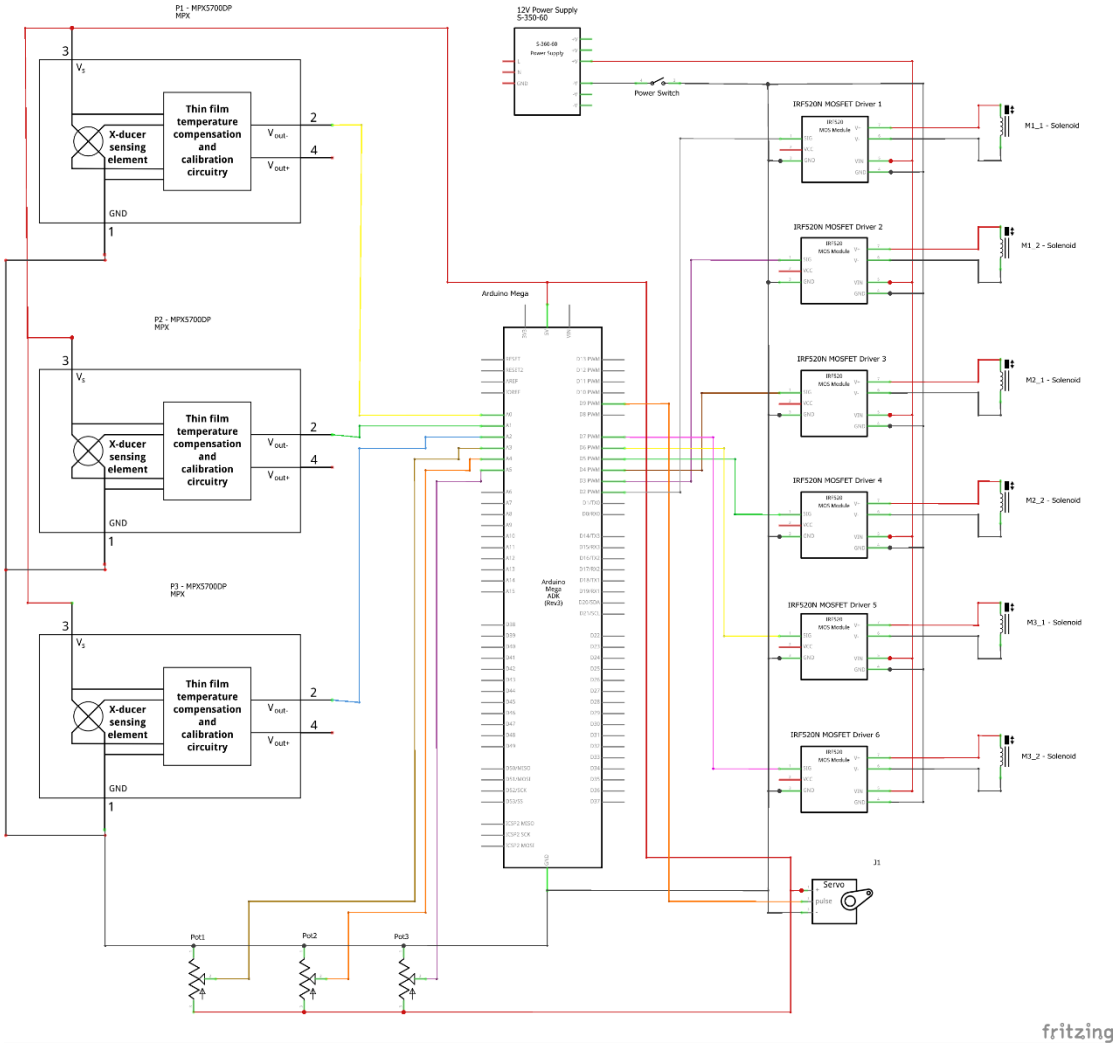

Figure 3.35 and 3.36 depicts the electrical connections of the control setup designed using Fritzing software utilized for this thesis while figure 3.37 depicts the hardware implementation. The MOSFET drivers were powered by the 12V power supply while the potentiometers, pressure sensors and SG90 servo motor were powered by the Arduino 5V line. The Arduino was powered by USB connection to the computer as it obtains pressure sensor values and sends commands through serial data communication.

Figure 3.37

Hardware Implementation of Electronic Circuit

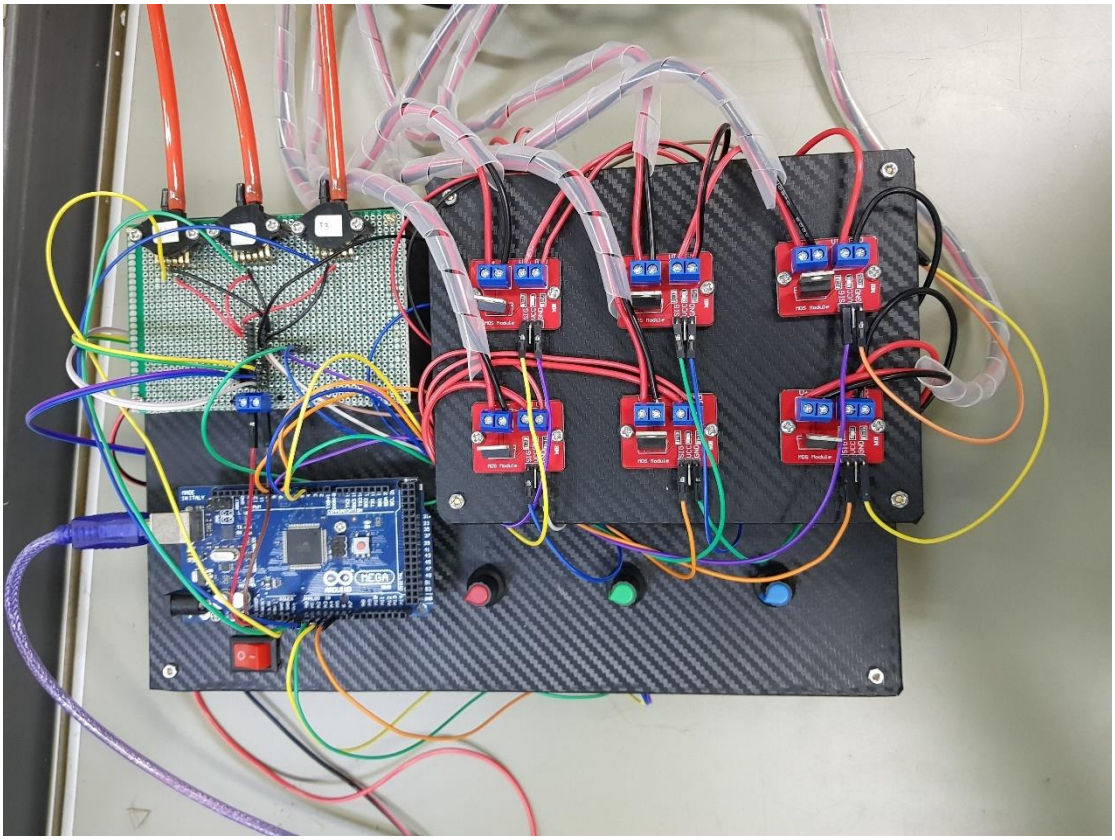

3.7 Control Structure

3.7.1 State Logic

The pneumatic hardware utilized in this thesis are ON/OFF solenoid valves. Thereby, it was necessary to develop a control system that suits the actuation of these valves. The robot actuator operates on three states,

1. Fill State: Fill valve is opened, and exhaust valve is closed
2. Hold State: Both valves are closed
3. Exhaust State: Fill valve is closed, and exhaust valve is opened

During the Fill State, air flows in and the actuator length increases. If necessary to hold the position (pressure) of the robot, the Hold State ensures that no air flows in or out of the actuator. If necessary to reduce pressure, the Exhaust State will allow air to flow out of the system. Although the actuators were tightly sealed, there is a possibility of small leakages. Thereby, in order to maintain pressure, a dead band 10kPa was introduced. This forces the controller output to adjust according to pressure overshoots

or leakages. Figure 3.38 depicts the state machine of the system where each actuator follows the logic individually (Booth et al., 2018).

Figure 3.38

State Machine Diagram

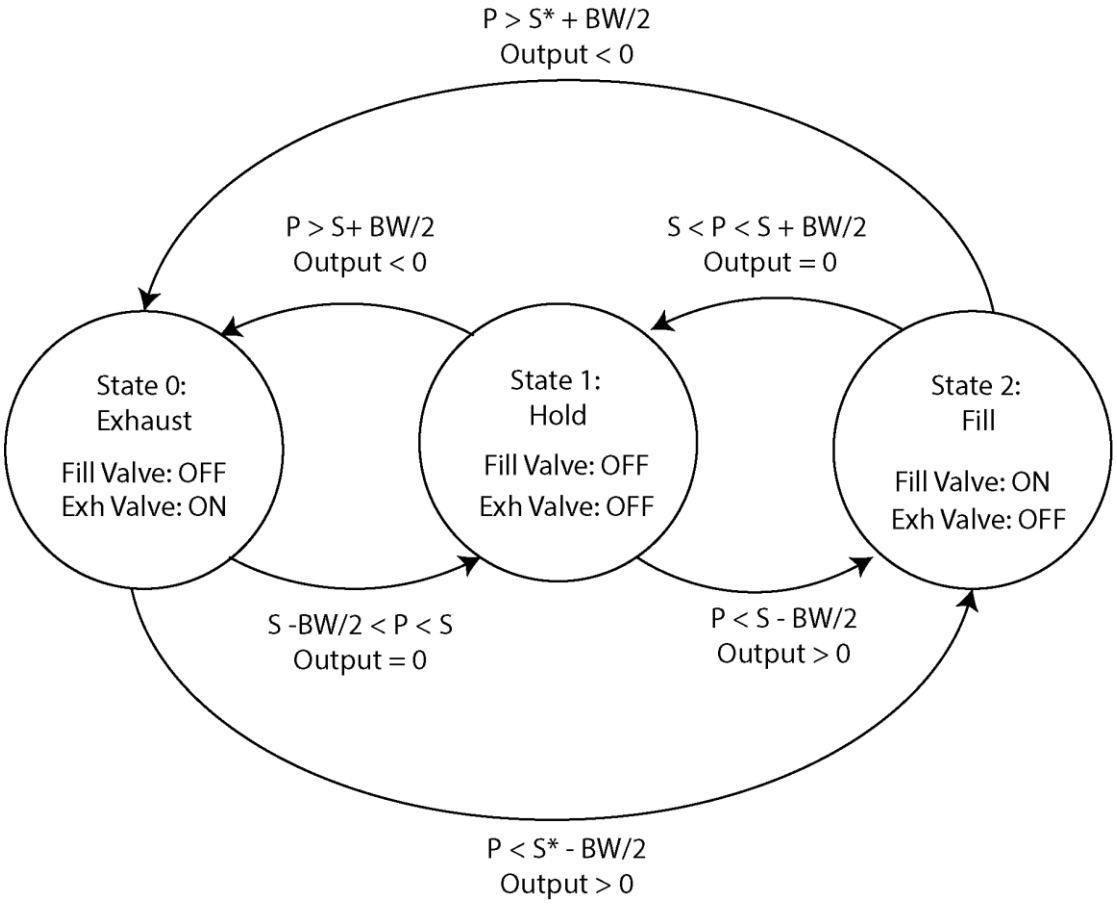

Where,

P = Pressure,

S = Setpoint,

BW = Dead-band Band Width (10kPa)

S* = New Setpoint

In this state machine it is necessary to note that the state transition from fill to exhaust and vice versa will occur if a new setpoint is defined during the current exhaust or fill state. The controller will try to maintain the pressure in the hold state. Due to pressure overshoots or leakages, the controller may try to exhaust or fill respectively.

3.7.2 PID Based Pressure Control

Rather than using a simple Hysteresis Controller (Bang-Bang Controller), it was decided to use PID control to control the output signal that will be fed into the state machine logic. Figure 3.39 depicts the PID loop utilized in this thesis (Young et al., 2019).

Figure 3.39

PID Control

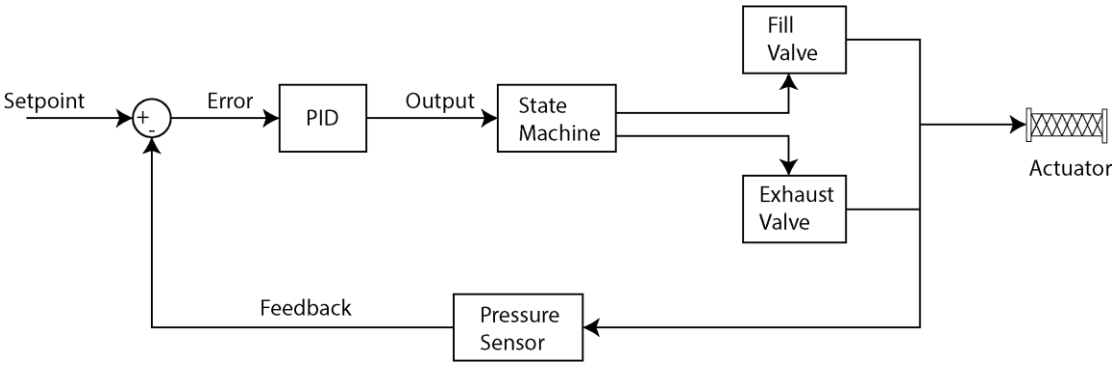

Where,

$$Error\ (e) = Setpoint - Pressure\ Feedback \tag{43}$$

$$PID = P + I + D \tag{44}$$

$$P = k_p e(t) \tag{45}$$

$$I = k_i \int e\,(t)dt \tag{46}$$

$$D = k_d \frac{d(e(t))}{dt} \tag{47}$$

In order to improve performance, the derivative was subjected to a low pass filter with time constant 0.02 to reduce high frequency noise. Furthermore, integrator anti-windup was implemented to avoid output saturation. Output was limited to a range of [-10,10] as the state machine is only concerned whether the output is positive, negative or zero and not the value. A sample time of 100ms was used to run the PID loop. This PID control loop was applied to maintain the pressure in the actuator. The position control was done separately.

3.7.3 Position Control

After pressure control is setup, it is necessary to utilize it to control the position of the robot. Position control was carried out in two ways: Manual setpoint input and Look-Up Table recordings. The analog potentiometer value was read by the microcontroller and was mapped to the working pressure range. The 10bit ADC resolution provides a range of 0 to 1023 which was mapped to 0 to 120kPa. Figure 3.40 depicts the anticipated end effector position in the x-y plane with the pressurization of each actuator.

Figure 3.40

Robot Actuation in X-Y Plane

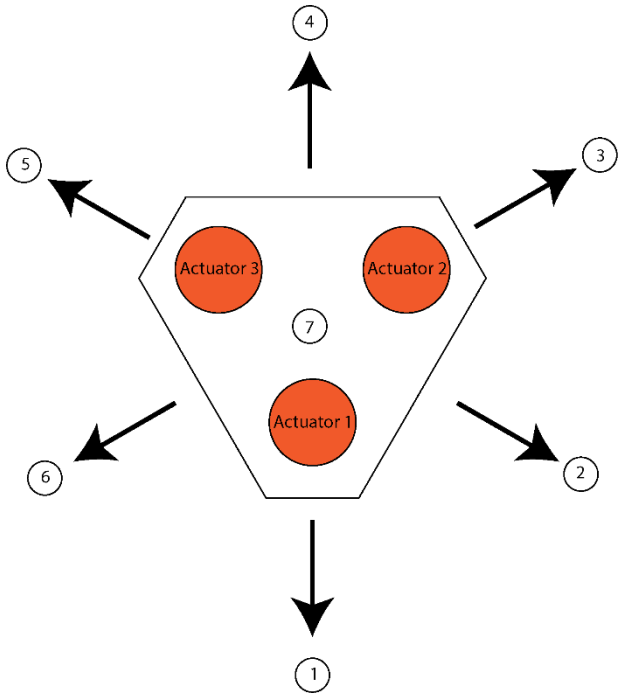

Figure 3.40 is a general map of directions the robot moves in the x-y plane when selective actuators are pressurized. Depending on the pressure values, the exact position of the robot will vary. The z position too depends on sequence and pressure. Higher pressures cause the robot to move higher upwards. Table 3.2 describes the sequence of pressures in the actuators with respect to the direction. Chapter 4 describes the results of manual setpoint input and the lookup table.

Table 3.2

Robot Actuation Description

Direction	Pressure State (High/Low)		
	Actuator 1	Actuator 2	Actuator 3
1	Low	High	High
2	Low	Low	High
3	High	Low	High
4	High	Low	Low
5	High	High	Low
6	Low	High	Low
7	High	High	High

Note. Direction 7 points outwards and along the z-axis.

CHAPTER 4
RESULTS

4.1 PID Tuning

PID tuning was conducted manually by observing the pressure response with respect to the setpoint as per the Arduino Serial Plotter data. The PID gains were tuned with step-by-step increments in k_p, k_i and k_d (Lynch Kevin, 2015). Despite the sealing of the pneumatic circuit, a minute amount of leakage is observed in the system. Thereby, during the Hold State, the pressure drops below the dead-band and forces the controller to provide a positive output. This may provide an oscillatory experience for the actuator hold state. This situation was not observed in the Fill and Exhaust States as they strive to increase or decrease the pressure up to the setpoint rather than maintain the pressure.

Thereby, the controller must be tuned enough to reduce the oscillations that may arise in attempting to reach a certain pressure. When the controller is too aggressive, i.e., excessive proportional gain increment, the pressure overshoots the setpoint which causes rapid state switching between Fill and Exhaust states as shown in figure 4.1.

Figure 4.1

Actuator Response with k_p =1000, k_i =0, k_d =0

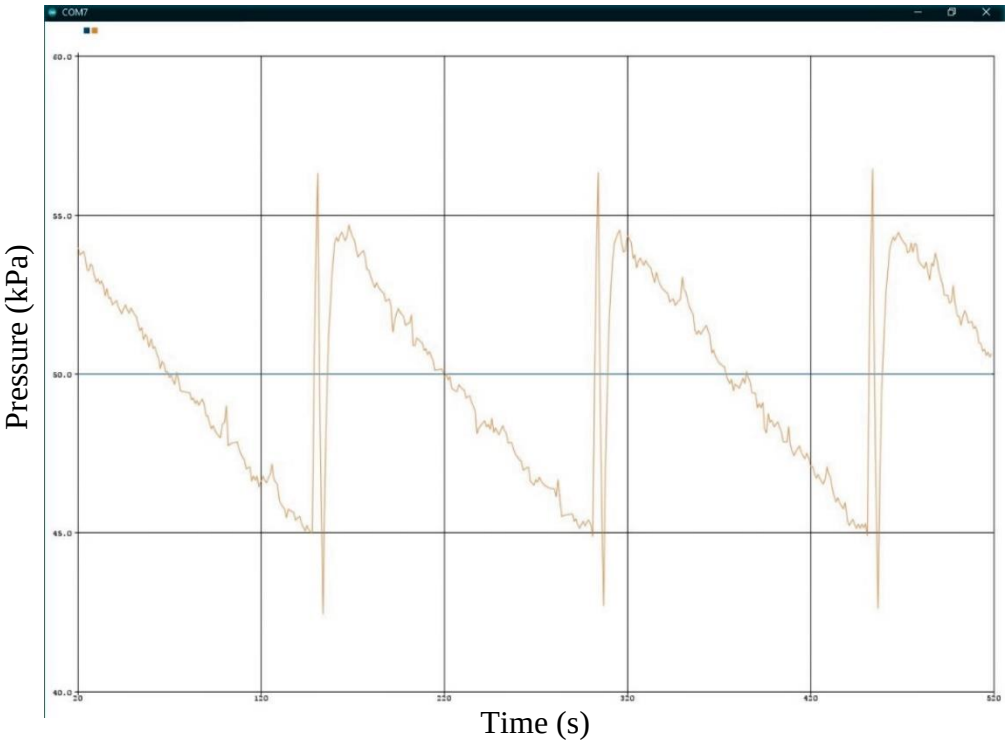

In figure 4.1, the setpoint is 50kPa with a dead-band of 10kPa, i.e., pressure must be maintained between 45-55kPa. The main goal was to remove rapid state switches to maintain the pressure between the dead-band. Since the system is consistent in achieving the dead-band pressure range, the integral term did not have much effect to reduce the error. However, excessive increments of the derivative term were not effective in dampening the oscillation between the states as shown in figure 4.2.

Figure 4.2

Actuator Response with k_p =200, k_i =10, k_d = 2000

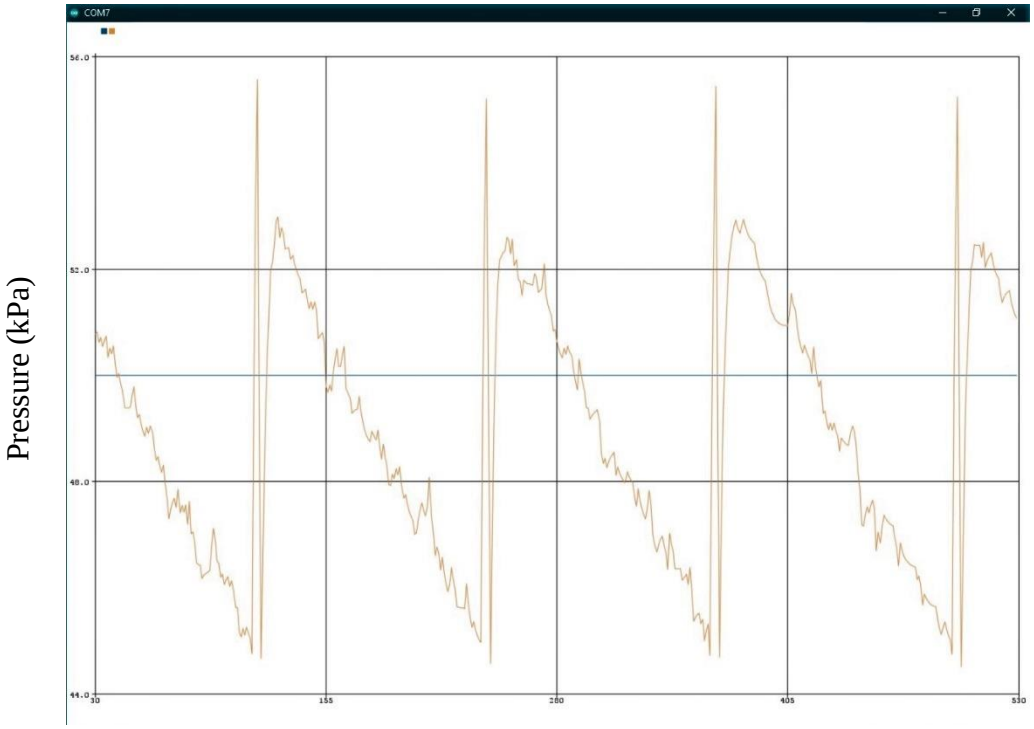

Through several intuitive adjustments based on the tuning process, the most favourable actuator response was recorded when the PID gains were k_p = 200, k_i = 5, k_d = 1000. These gain values allow the controller to increase the controller without overshoot which also avoids rapid state switching as shown in figure 4.3. Thereby, the controller could maintain the pressure against the leakages.

However, it must be noted that the Hold state is not perfect as the controller tries to maintain the pressure. Opening of the fill valve causes sudden pressure increments which produces jerking movements in the actuator. With the optimum gain values, this

effect was minimized as there are no rapid state changes and the time between adjustments was maximized. Furthermore, these gain values proved to be suitable for all three actuators.

Figure 4.3

Actuator Response with k_p =200, k_i =5, k_d = 1000

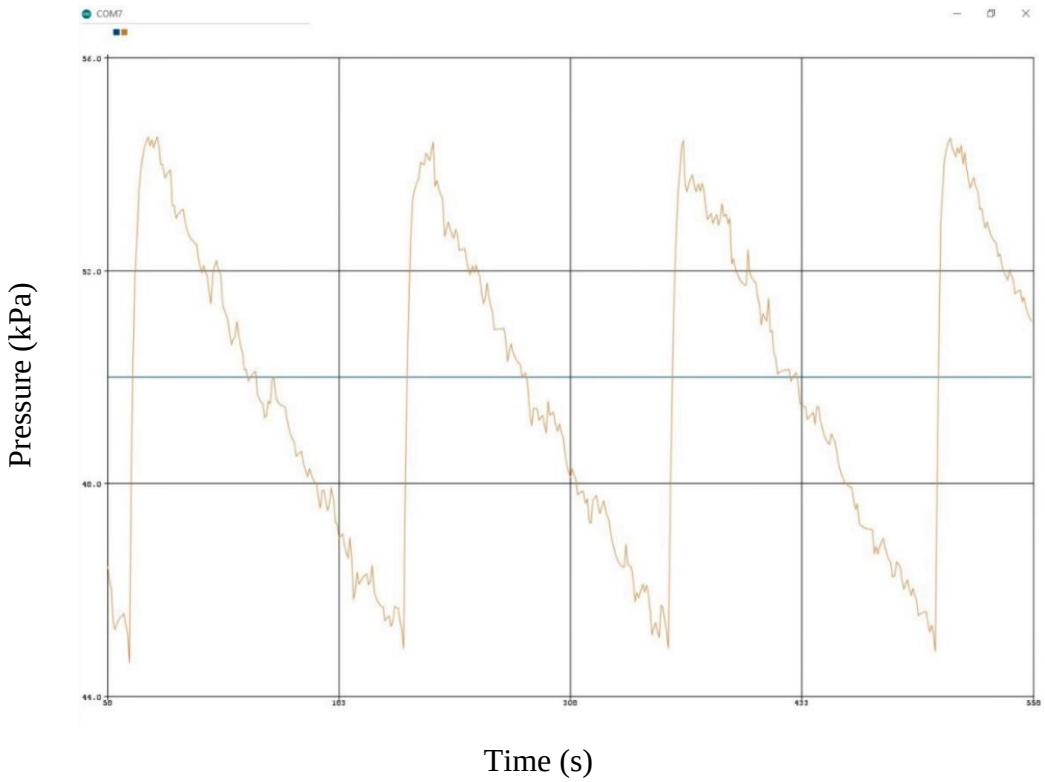

4.2 Manual Pressure Setpoint

The robot control electronics were designed such that the user can provide manual pressure setpoints to control the robot position open loop. As discussed in section 3.7.3, the potentiometer analog readings were mapped to pressures ranging from 0-120kPa. As the safety limit is 125kPa, the controller ensures that the actuator does not exceed the pressure limits.

This feature allows the user to interchangeably vary the three pressure values test the position of the robot. Figure 4.4 depicts the response of a single actuator by changing the setpoint manually. Figure 4.5 depicts the response of two actuators when setpoints were changed manually. The irregularity in the middle portion of the graph is due to random noise in the potentiometers. Figure 4.5 depicts the response when all three

actuators are provided setpoint changes. Throughout these graphs, it can be noted that the PID loop performs well, and the robot responds well to pressure changes.

Figure 4.4

Single Actuator Response with Setpoint Changes

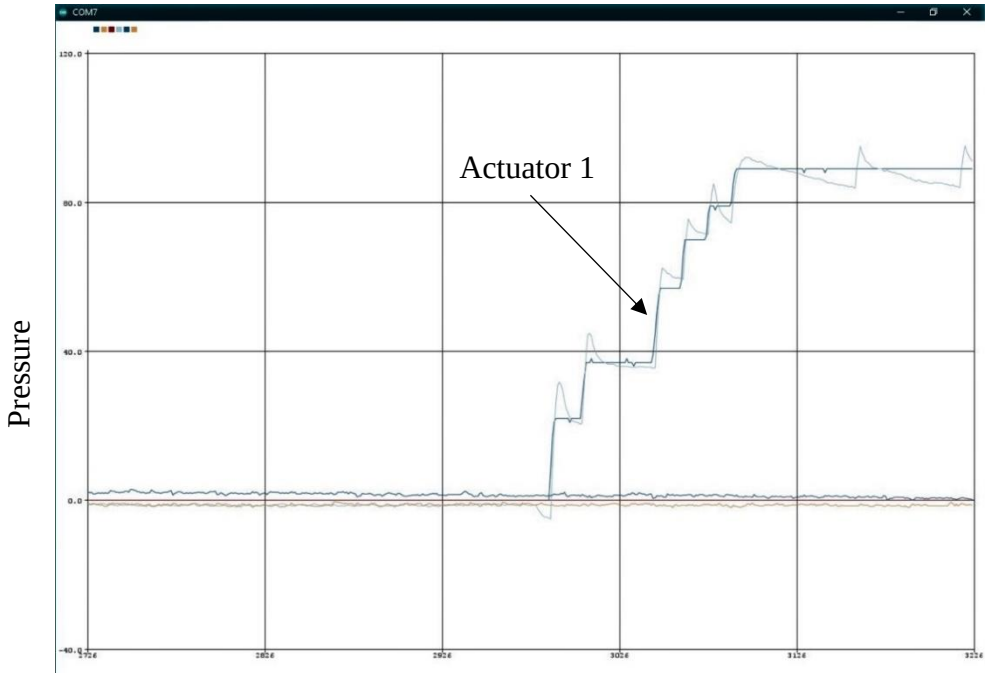

Figure 4.5

Response for Two Actuators with Setpoint Changes

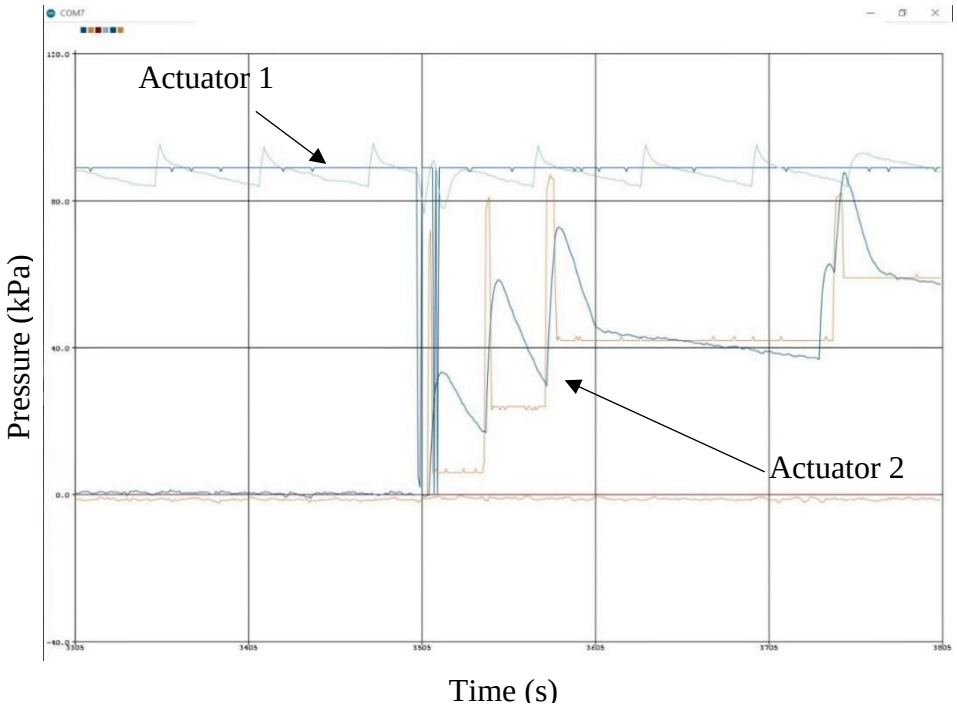

Figure 4.6

Response for All Three Actuators with Setpoint Changes

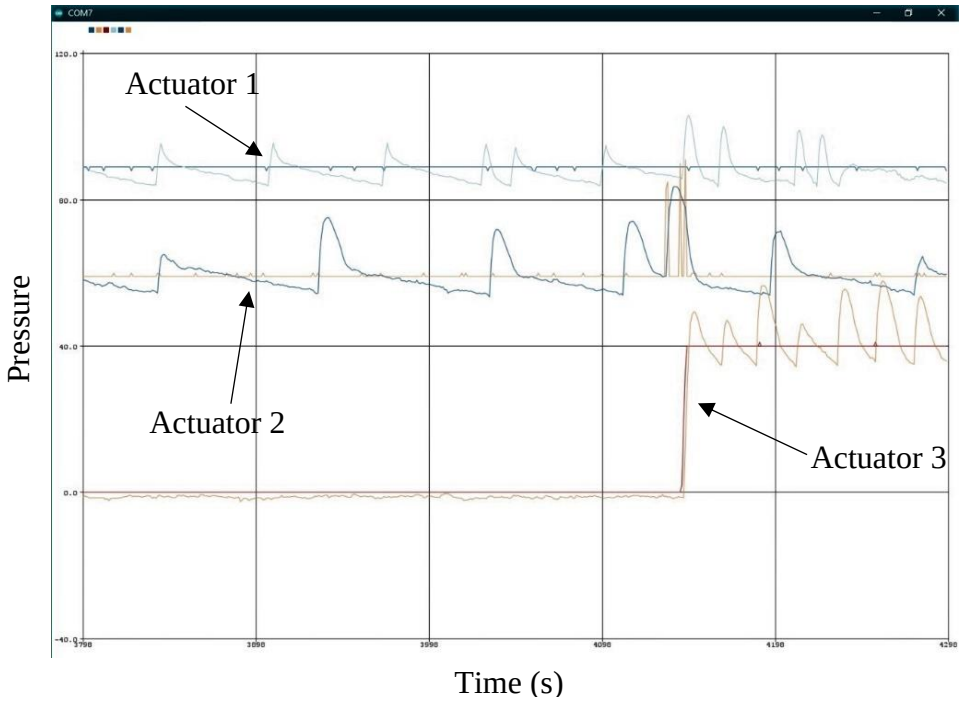

4.3 Look-Up Table (LUT)

The objective of this thesis requires position control and to verify that the robot would operate within specification goals. To achieve this, a Look-Up Table was used to record the robot position with respect to the pressure setpoints. Thereby, the robot setup was modified to include 1cm grid paper in the planes x-y, y-z, and x-z as shown in figure 4.6.

Due to practical reasons, the origin of the measurement space was set in a corner of the aluminium frame. The z position contains an offset due to the thickness of the endcaps and end effector plates. However, the final recordings were adjusted with respect to the base and end effector of the robot as defined in kinematic model developed in section 3.2. The position was noted on the graph paper with the use of a taught string. Furthermore, the lengths of the robot's actuators were noted down for each position to verify with the simulation result.

For this purpose, combinations of zero pressure, full range (120kPa ± 5kPa) and half range (60kPa ± 5kPa) pressures were utilized. See Appendix for the measurements

obtained from the experiment as well as the adjusted measurements considering the base position, orientation and z offset.

Figure 4.7

Position Measurement Setup

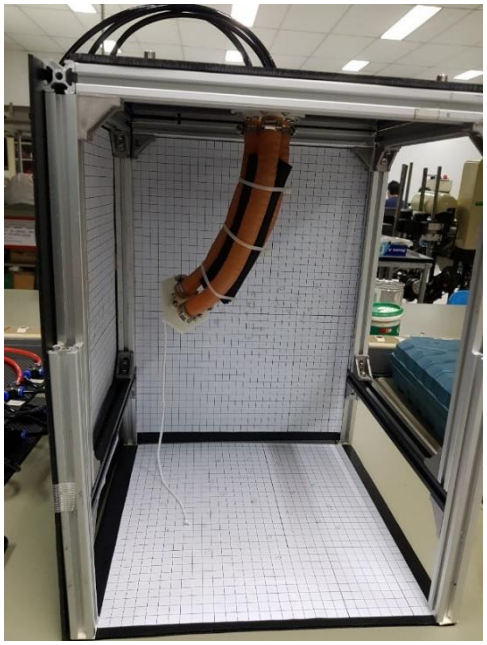

Figure 4.8

Robot Position Measurement for Y-Z

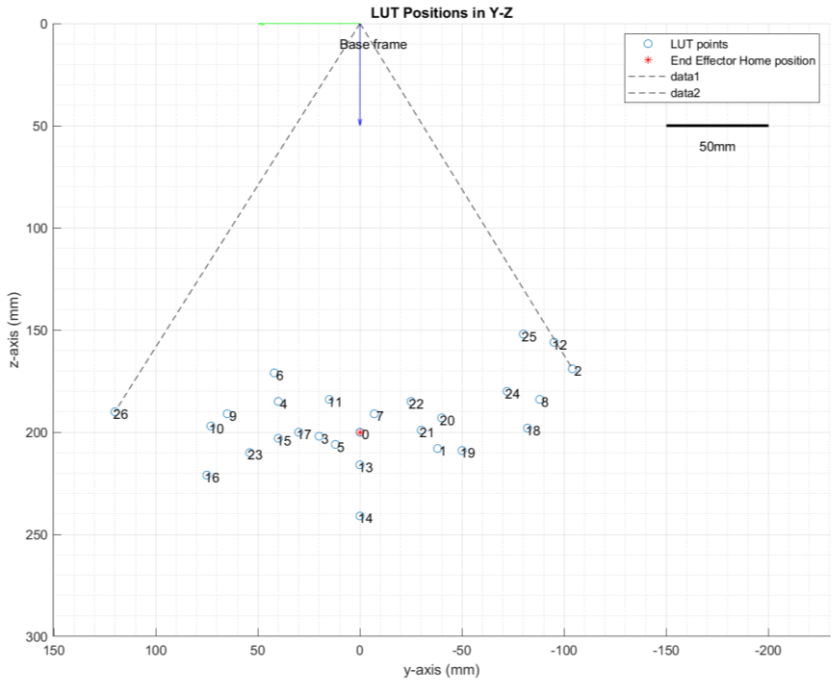

Figure 4.9

Robot Position Measurement for X-Z

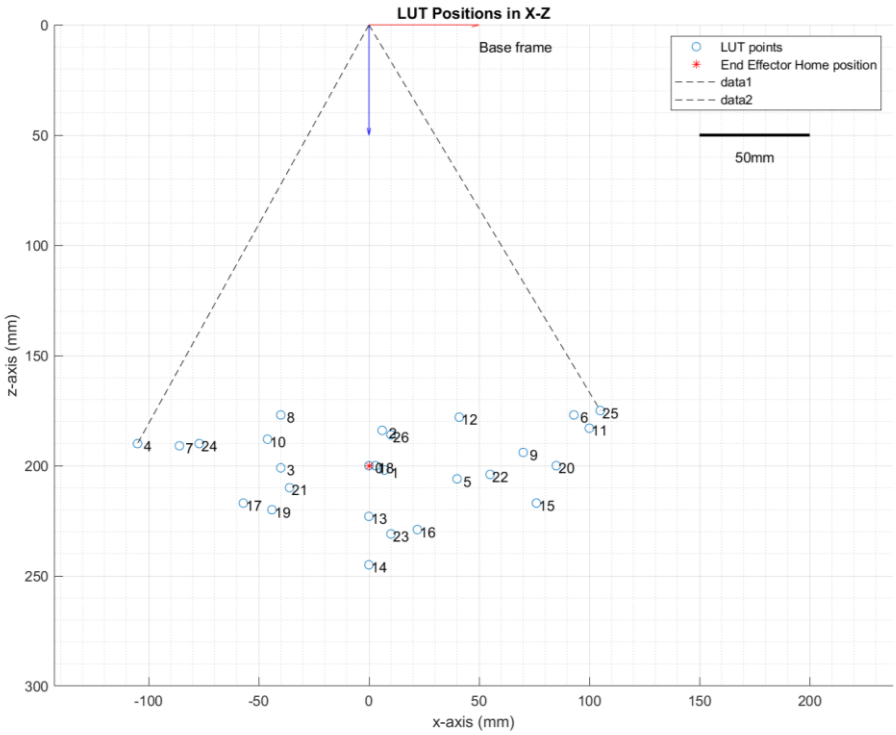

Figure 4.10

Robot Position Measurement for X-Y

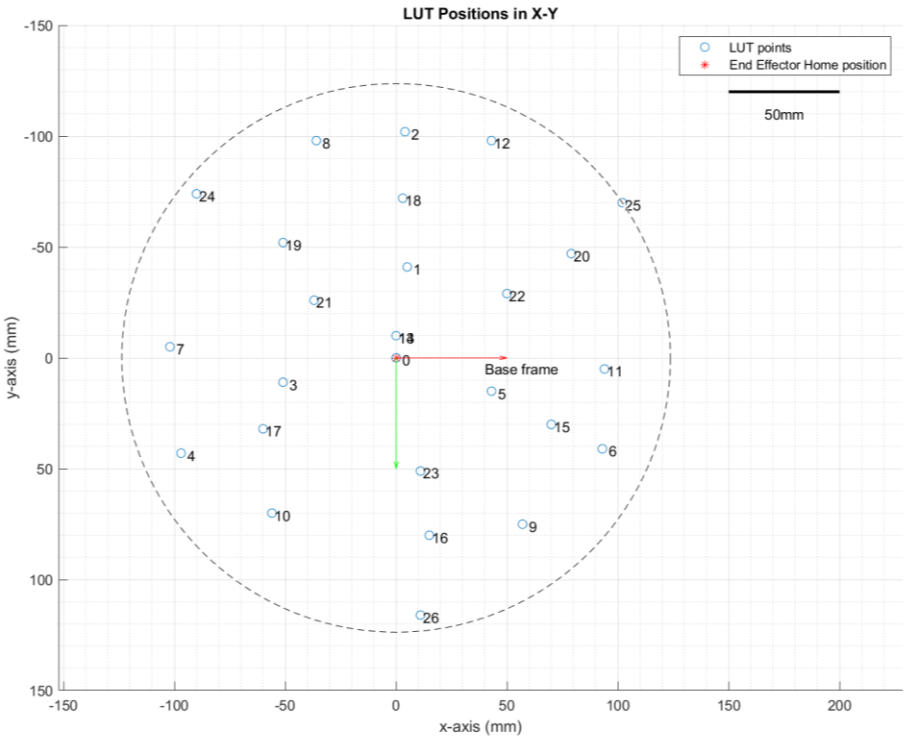

Figures 4.8, 4.9 and 4.10 provides the robot position scatter plots for y-z, x-z and x-y planes. From figure 4.8 and 4.9, the dotted lines depict the variation angle of the working space covered by the robot. Considering the y-z plot where the furthest points are number 2 and 26, as well as the x-z plot's points 4 and 25, the following calculation can be done to verify the maximum variation angle that the robot achieves (See Appendix for the point locations). The resulting value is greater than the value suggested in the scope of this thesis.

$$y - z\ location\ of\ point\ 26 = (120{,}190)$$
$$y - z\ location\ of\ point\ 2 = (-104{,}169)$$
$$x - z\ location\ of\ point\ 4 = (105{,}190)$$
$$x - z\ location\ of\ point\ 25 = (-105{,}190)$$

Depicting the above coordinates as a set of triangles as in figure 4.11,

Figure 4.11

Calculation of Variation Angle with Respect to Y-Z and X-Z Plots

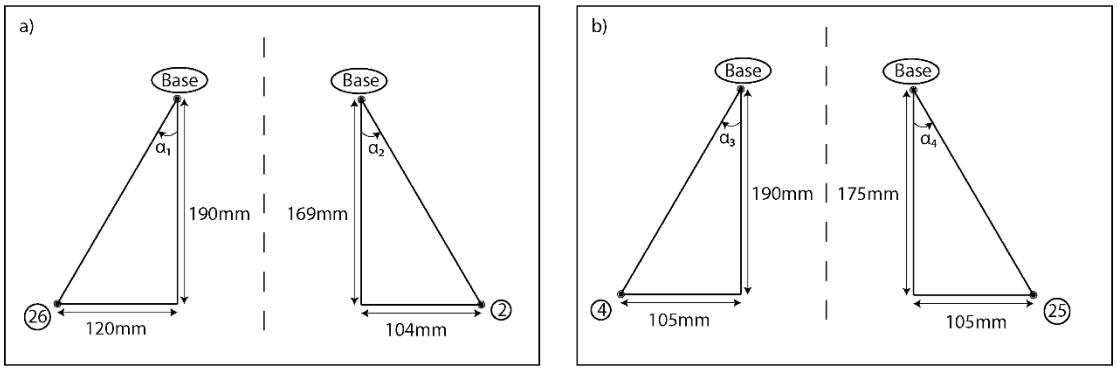

$$\alpha_1 = \tan^{-1}\left(\frac{120}{190}\right) = 32.28^o$$
$$\alpha_2 = \tan^{-1}\left(\frac{104}{169}\right) = 31.61^o$$
$$\alpha_3 = \tan^{-1}\left(\frac{105}{190}\right) = 28.93^o$$
$$\alpha_4 = \tan^{-1}\left(\frac{105}{175}\right) = 30.96^o$$

Maximum average variation angle,

$$\alpha_{ave} = \frac{32.28^o + 31.61^o + 28.93^o + 30.96^o}{4} = 30.945^o \approx 31^o$$

Figure 4.9 provides the largest area covered in the x-y plane which encircles end effector home position to the farthest point reached by the robot in the x-y plane. The radius of this circle was measured to be 123.7mm as observed in figure 4.10. Thereby, this thesis exceeded the requirements of the scope as the robot has a working space of a hemispherical area of radius 12.37cm with variation angle 31º.

Figure 4.12

Robot Position Measurement for X-Y-Z

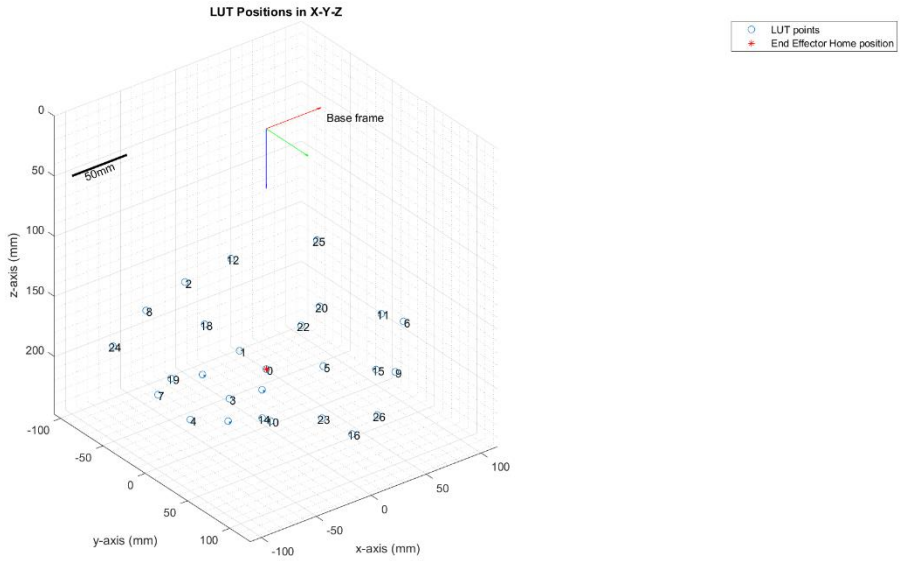

Figure 4.12 depicts the 3D position of the robot in x-y-z space with respect the base frame. Figures 4.13, 4.14, 4.15 and 4.16 depicts the comparison between the simulation versus the experimental results for y-z, x-z, x-y planes, and x-y-z 3D space respectively. In all the figures, the position 0 represents the home position of the end effector, i.e., when none of the actuators are pressurized.

Figure 4.13

Robot Position Measurement vs Simulation Results in Y-Z

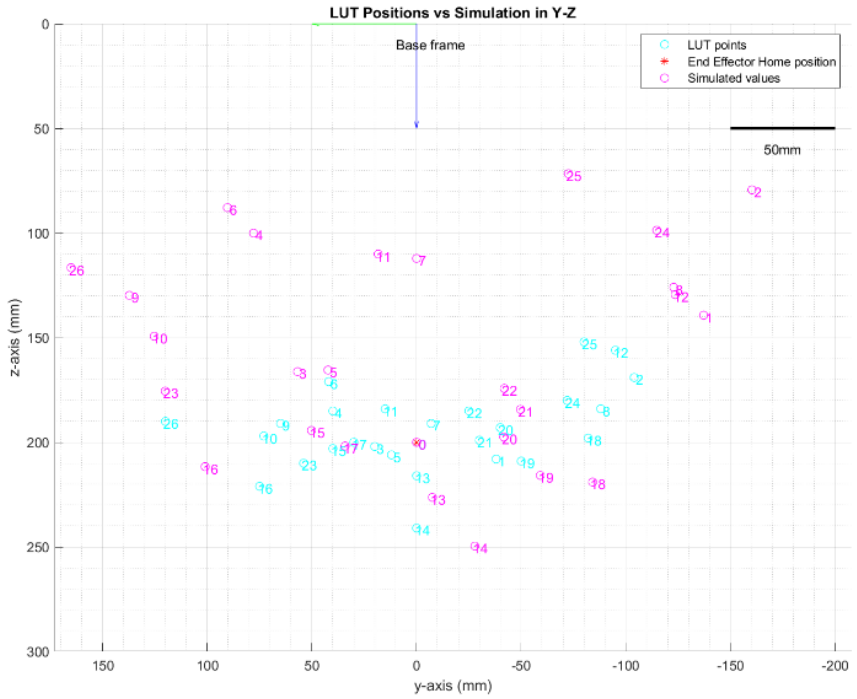

Figure 4.14

Robot Position Measurement vs Simulation Results in X-Z

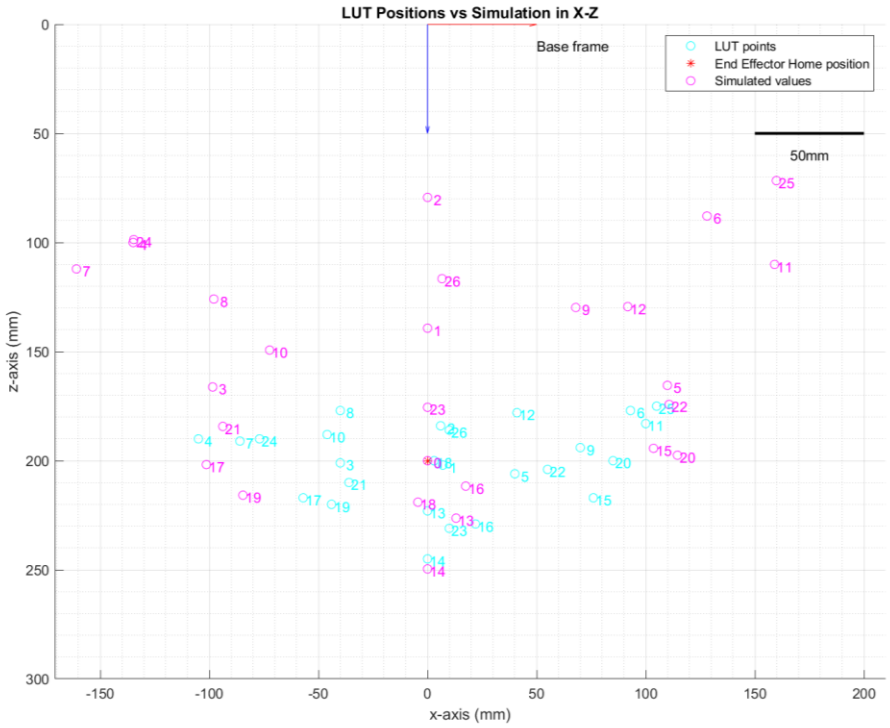

Figure 4.15

Robot Position Measurement vs Simulation Results in X-Y

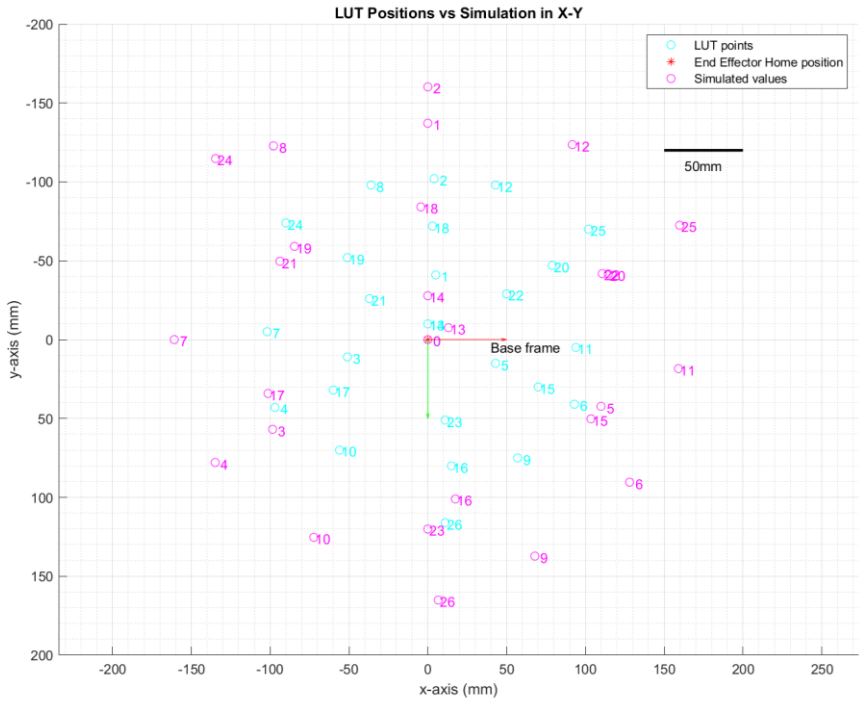

Figure 4.16

Robot Position Measurement vs Simulation Results in X-Y-Z

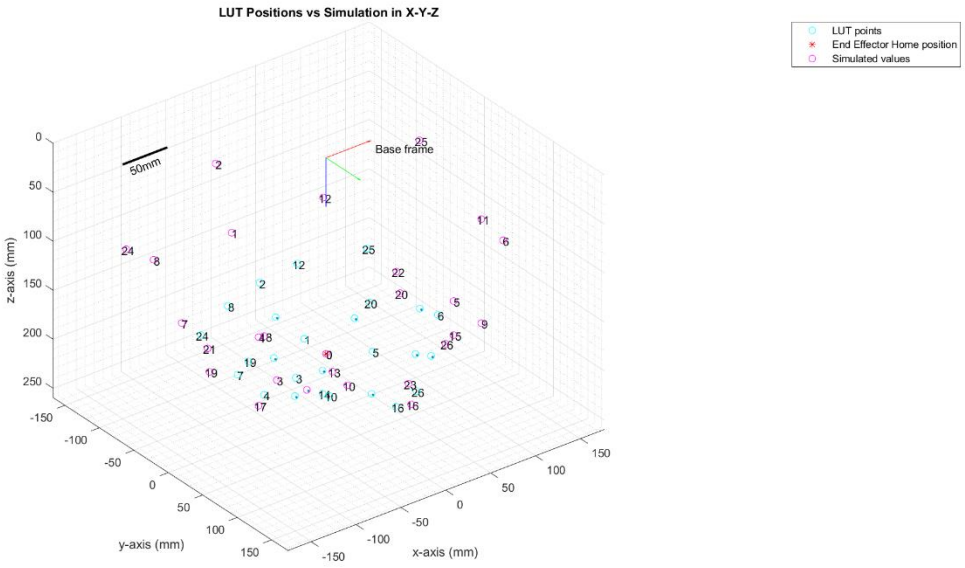

It must be noted that the measured results may have measurement errors as the method of measurement is not completely precise. From the comparisons in the above figures, it can be noted that some of the measured points are closely located with respect to the simulated results and follow the same direction patterns.

Figure 4.17 provides the error associated with the position measurement compared to the simulation result. Large error values can be observed within the position points 1-13 and 21-26. The range of points 13-20 contain relatively smaller errors around. Referring to the appendix table A1, it can be noted that the all the points that show large errors has at least one un-actuated actuator, while in points 13-20 all 3 actuators have been pressurized with a full range or half range pressure combination.

Figure 4.17

Robot Position Error

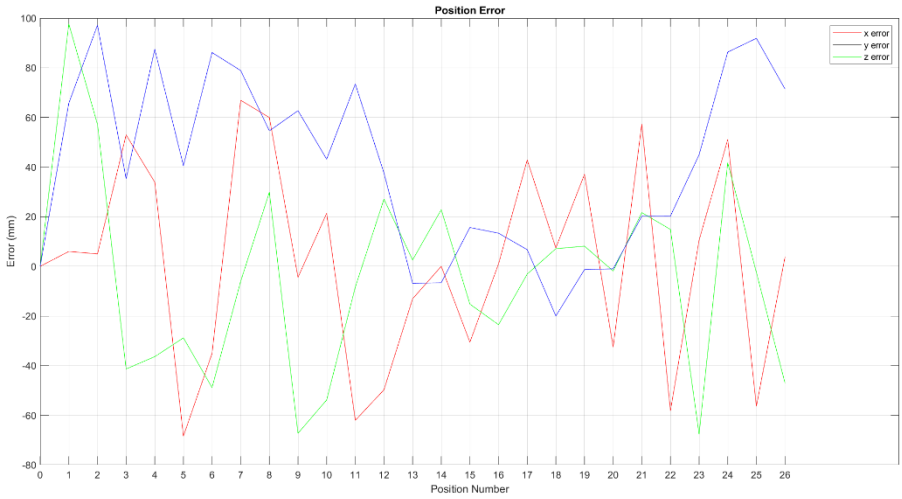

The error in general may be attributed to high non-linearity of the robot with respect to the materials and actuation method used. Although the kinematics of the robot are somewhat useful in providing a perception of the general direction and position of the robot, it is does not precisely capture the non-linear behaviour of the robot. Thereby, this robot will be utilized to operate within the recorded points of the Look-Up-Table as demonstrated in the section 4.4. Further improvements will be discussed in chapter 5.

4.4 Pick and Place Operation

In order to perform positioning operations, the respective Look-Up-Table points were coded as arrays containing pressure setpoints, position data, and robot length data in the robot software. The index of each array refers to the respective position and can be used to refer to all position data and display when the robot is commanded to move a certain position. The position command is sent to the microcontroller via serial communication by typing in the desired position number (0-26). This number will be cross referenced through all the arrays and display the position data as shown in figure 4.17 where LUT point 24 is called through serial monitor.

Figure 4.18

Serial Communication Data for Point 24

S1	S2	S3	M1	M2	M3	x	y	z	l1	l2	l3
120.00	120.00	0.00	122.17	119.48	3.67	-8.35	-7.30	21.50	26.70	25.70	21.50
120.00	120.00	0.00	121.76	119.19	3.49	-8.35	-7.30	21.50	26.70	25.70	21.50
120.00	120.00	0.00	121.70	118.99	3.36	-8.35	-7.30	21.50	26.70	25.70	21.50
120.00	120.00	0.00	121.66	118.39	3.73	-8.35	-7.30	21.50	26.70	25.70	21.50
120.00	120.00	0.00	121.63	118.43	3.76	-8.35	-7.30	21.50	26.70	25.70	21.50
120.00	120.00	0.00	121.61	118.46	3.55	-8.35	-7.30	21.50	26.70	25.70	21.50
120.00	120.00	0.00	121.59	118.48	3.64	-8.35	-7.30	21.50	26.70	25.70	21.50
120.00	120.00	0.00	121.35	118.49	3.47	-8.35	-7.30	21.50	26.70	25.70	21.50
120.00	120.00	0.00	121.19	118.27	3.80	-8.35	-7.30	21.50	26.70	25.70	21.50
120.00	120.00	0.00	121.30	118.57	4.04	-8.35	-7.30	21.50	26.70	25.70	21.50
120.00	120.00	0.00	121.38	118.33	3.75	-8.35	-7.30	21.50	26.70	25.70	21.50
120.00	120.00	0.00	121.43	118.16	3.54	-8.35	-7.30	21.50	26.70	25.70	21.50
120.00	120.00	0.00	121.24	117.81	3.63	-8.35	-7.30	21.50	26.70	25.70	21.50

Here, S1, S2, and S3 refers to the setpoints, M1, M2, and M3 refers to the measured pressure values, x, y, z, l1, l2, and l3 refers to the LUT data of cartesian positions and lengths of actuators. It can be noted that the system tries to maintain the pressure well within the dead-band of the setpoint as intended. Thereby, moving the end effector to the pre-recorded position.

For the purpose of gripping objects, a string is passed along with the position number integer. The character “o” rotates the servo motor by 30^{o} opening the jaws, “c” by 98^{o} closing the jaws and “g” by 80^{o} providing and intermediate open jaw position. Hence the robot program recognizes the string to command the servo motor to open or close the jaws of the gripper. The number in the command is parsed as an integer and cross referenced to each of the LUT arrays.

For example, the command “c24” refers to close gripper at position 24 and “o11” refers to open gripper at position 11. Thereby, it is possible to open and close the gripper at specific positions allowing the robot to grab objects as shown in figure 4.18 and 4.19.

Figure 4.19

Robot Picking an Object at Position 14 and Placing at 2

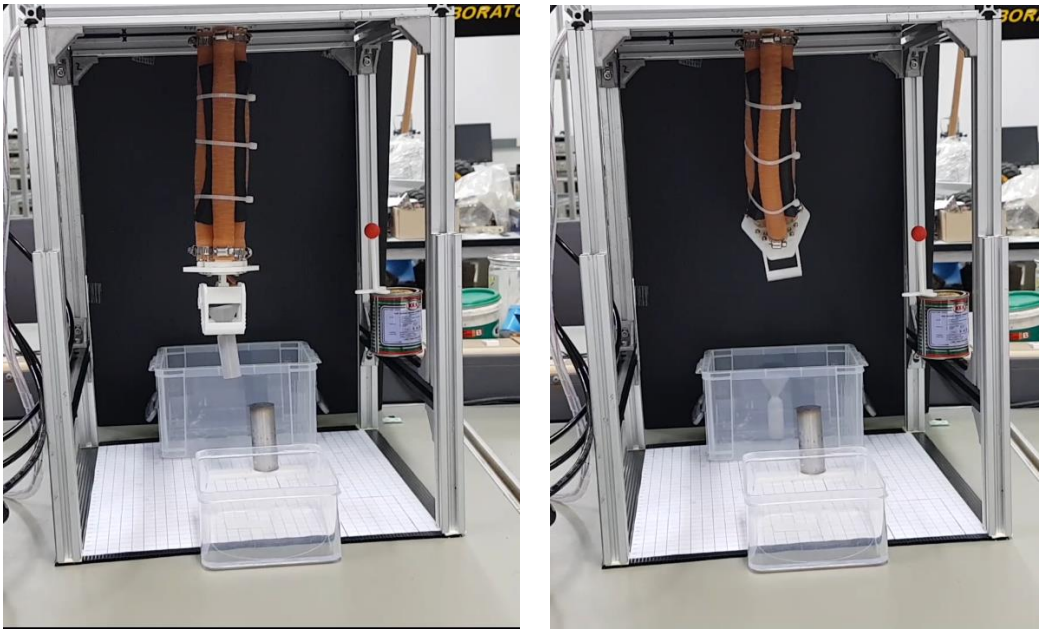

Figure 4.20

Robot Picking an Object at Position 11 and Placing at 26

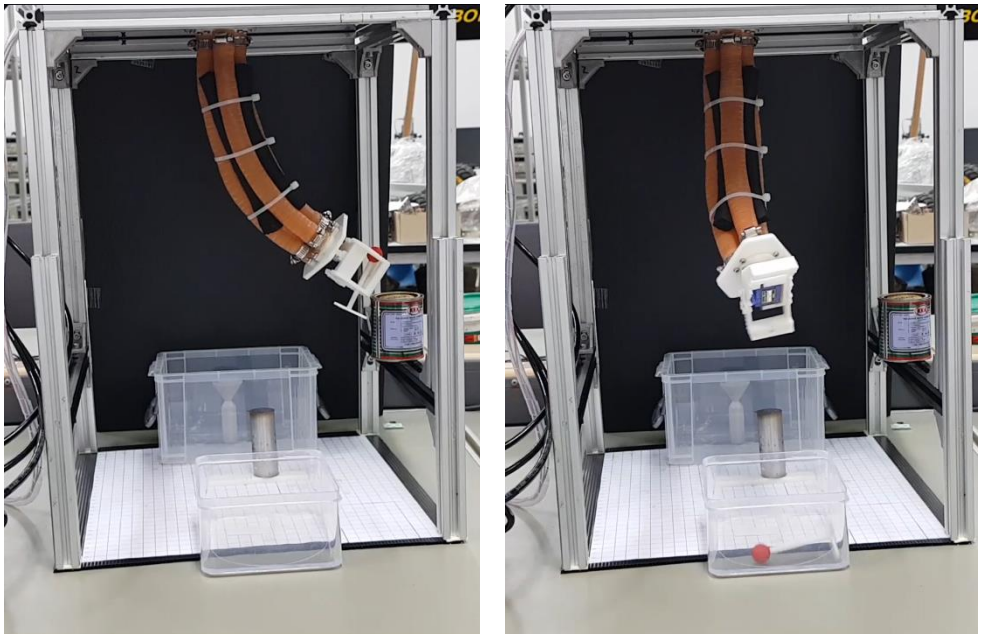

4.5 Manipulator Response Time

Delta Robots are designed to be fast actuating mechanisms. However, in this thesis the speed of the robot had to be reduced up to a certain degree to avoid damage and failure of the actuators. This is because the ON/OFF solenoid valve actuation can cause impulsive increments of the pressure that may exceed the safety limit of the actuators. Figure 4.21 depicts the response time of a single actuator with respect to 10kPa pressure increments.

Figure 4.21

Response for a Single Actuator with 10kPa Pressure Increments

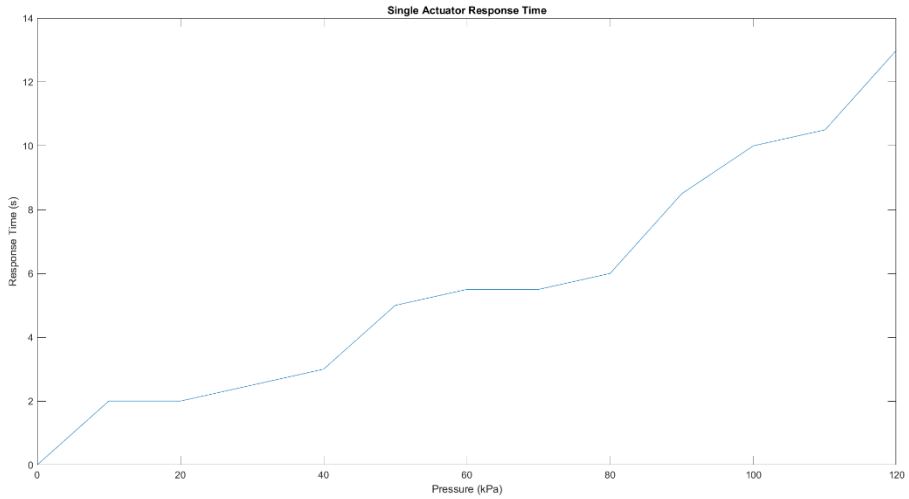

The experiment observed the response time for pressures of actuator increased from 0kPa. As can be observed from the graph, the response time too increased when the required pressure setpoint increased. This is because of the time taken by air to fill up the tube up to the respective pressure. The result is not exactly linear as pneumatic pressure is non-linear. However, the gradual increments of response time can be expected with this setup.

Figure 4.22 depicts the response times for each actuator to reach the pressure setpoint for each recorded position. The graph provides insight as to how the response time varies with different actuator pressurization combinations. The response time is greater when multiple actuators are pressurized. In scenarios with response times greater than 10s, the actuators were pressurized at full range pressure.

Figure 4.22

Actuator Response for a LUT Positions

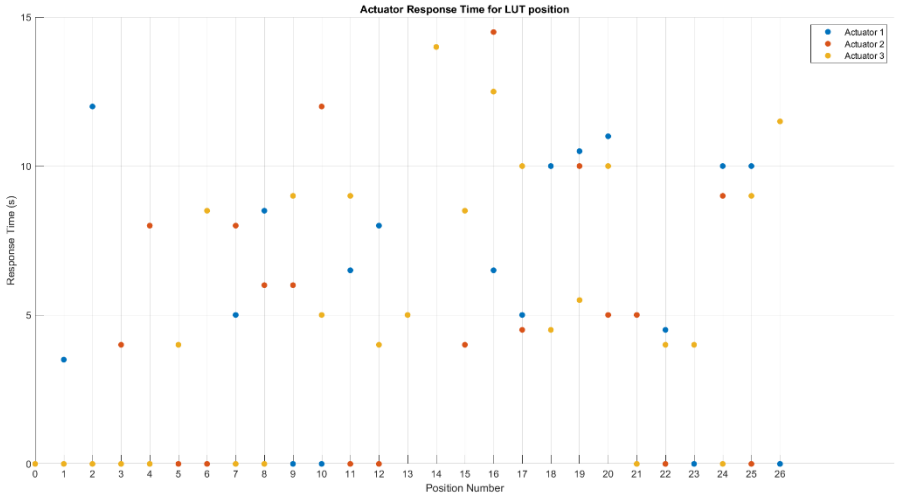

Figure 4.23

Manipulator Response for a LUT Positions

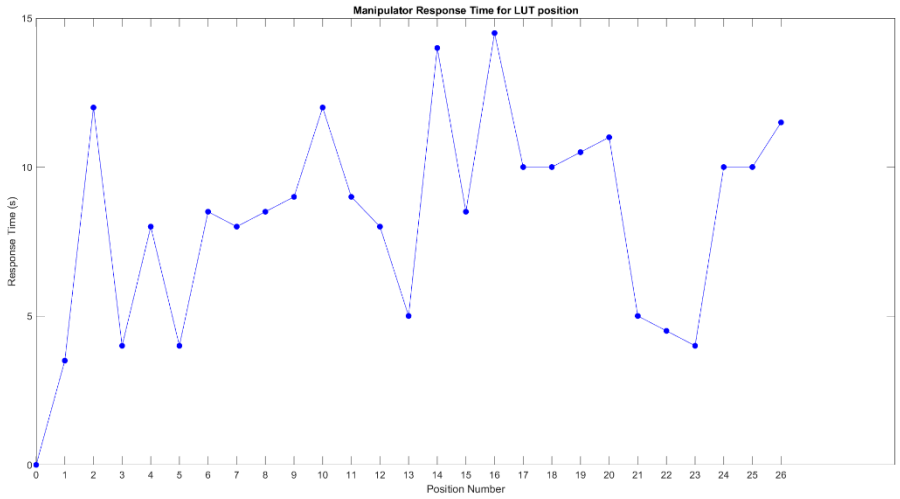

Figure 4.23 depicts the response time for the entire manipulator to reach a specified position. This graph considers the response time for the longest duration consumed by actuators as the final value of the manipulator response time, i.e., when the manipulator finally reaches the specified position. Positions that require full range pressures consumes the most amount of time. Even with the non-linear nature of pneumatic actuation, the results provide clear insight on the response time variation.

4.6 Manipulator Load Capacity

Further testing was carried out to observe the behaviour of the robot when external loads were applied to the end effector of the robot. Figure 4.24, 4.25, and 4.26 depicts the variation of error of the position changes with the incremental addition of weights in x, y, and z directions respectively.

Figure 4.24

Absolute Error in X Direction vs Load

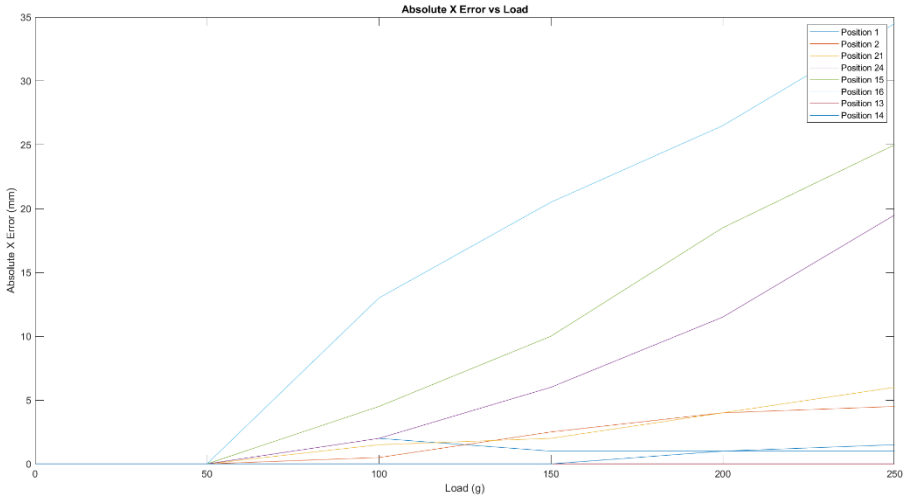

Figure 4.25

Absolute Error in Y Direction vs Load

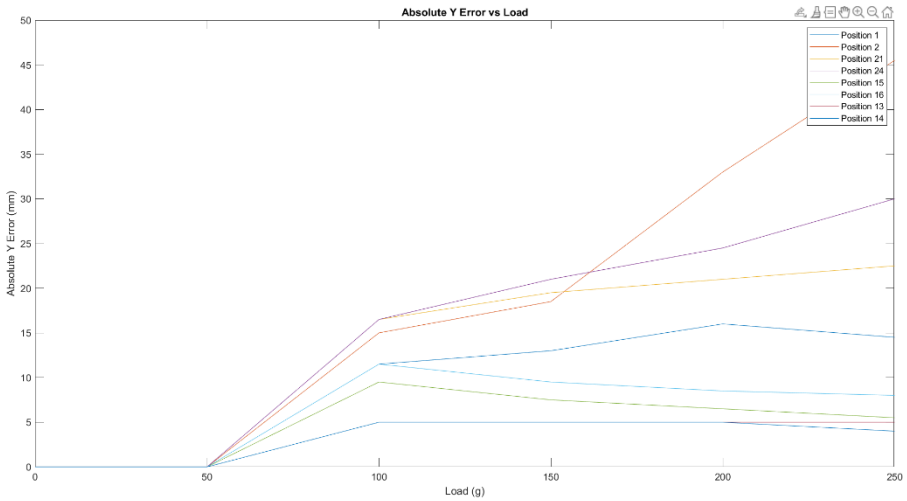

Figure 4.26

Absolute Error in Z Direction vs Load

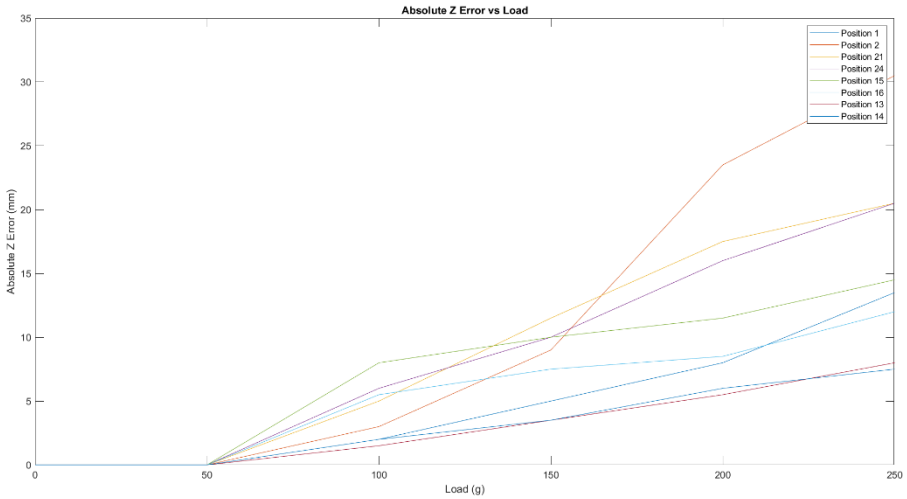

For the purpose of this experiment, only a select few positions were considered. These positions contain a variety of pressure combinations that reflect on how the loading affects the positioning with respect to the pressure inside the actuator. As can be expected, the error greatly increases with further increments of weight. However, it can be noted that the error is greater when single actuator is pressurized. This is due to the manipulator not being able to provide adequate force to maintain the position.

Furthermore, single actuator at full range pressure, the manipulator seems to have higher error compared to the previous scenario. This may be caused by the potential to have higher error as the manipulator position is at a further distance from the home position and the single actuation even with higher pressure does not provide enough force output to carry the load.

At certain positions, the variation of error is not similar for each direction. This may be due to the non-linearities caused by pneumatic actuation, materials used and the oscillations due to pressure regulation. It was noted that increasing load caused the pressure regulation oscillations to magnify and was detrimental to the overall result.

CHAPTER 5
CONCLUSION

5.1 Conclusion

From the results provided in the previous chapter it is possible to come to many conclusions regarding this research project. The main goal of this thesis is to integrate a flexible actuator to a Delta type robot configuration. This was achieved through the use of a Reverse Pneumatic Artificial Muscle (RPAM). Although not the same in structure as a bellow type actuator, the RPAM is capable of extending its body with near linearity. This type of actuator is quite suitable for flexible actuation in a Delta Robot.

It is noteworthy to mention that the objectives of this thesis were met. The use of 3 RPAM actuators allowed the robot to move with 3 Degrees of Freedom (DOF). The RPAMs were designed and fabricated with easily accessible materials and processes that are convenient. Thus, it is possible recreate and replace these flexible actuators if any damage is sustained to the robot body. These actuators have the ability to change its length as per the requirements of the user. Furthermore, combining these actuators as a parallel linkage, provides bending action. With the pressure feedback from the actuators, it was possible to control the pressure within the robot thus providing access for position control of the robot.

This thesis was able to achieve the above objectives well within and above the scope and limitations proposed. The three RPAM actuators allowed 3DOF which allowed position control within the translational x-y-z axes. The feedback was obtained through MPX5700DP pressure sensors. The measurement data from those sensors were adequate in the position control of the robot. However, implementation of a vision system was not feasible with the current configuration and setup of the robot. The movement of the robot at certain poses obscures the field of view. Thereby, the setup of the robot has to be designed in way to allow the vision system to obtain better data.

Thereby, the robot utilizes a Look-Up-Table which contains the actuator pressure combinations to allow the robot to move to the required location through user

commands. Through this process, it was possible to exceed the scope proposed; the robot has a working environment of a hemisphere of radius 12.37cm with variation angle of 31^{o}.

The utilization of the ON/OFF solenoid valve pairs does not provide a smooth actuation profile as a proportional control valve. However, the current solenoid valve system provides an effective way of regulating pressure without exceeding budget constraints. Through the use and tuning of the PID controller, it was possible to minimize the actuation/de-actuation oscillations present in the robot system. The next section provides details on how this system can be improved for future research work.

5.2 Recommendations

1. Utilize proportional control valves to vary the pressure inside the actuators. Proportional valves in the market may be very expensive and may not be accessible. It is possible to motorize pneumatic throttle valves or speed controllers to proportionally regulate the airflow thus providing a customized proportional controller at a manageable cost.
2. Implement a robust vision system to provide information about position and orientation of the robot and even length changes of the actuators. IMU sensors may be used to provide more data for attitude control. This will provide better control for the robot which enables for practical usage of this type of robots.
3. Include additional robot sections and actuators per section. This will allow more degrees of freedom and provide the robots better reachability. However, this implementation requires greater insight into the dynamics and non-linearity imposed by the materials and actuation method.
4. Inclusion of a soft gripper to the robot adds more value to the flexible actuation. Furthermore, this type of gripper would minimize the electronics used on the robot body.
5. Conduct a study on the force control of the robot to optimize the robot controller to minimize its error when handling payloads.

REFERENCES

Al-Ibadi, A., Nefti-Meziani, S., Davis, S., & Theodoridis, T. (2018). Novel design and position control strategy of a soft robot arm. *Robotics*, *7*(4). https://doi.org/10.3390/robotics7040072

Andrikopoulos, G., Nikolakopoulos, G., & Manesis, S. (2013). Pneumatic artificial muscles: A switching Model Predictive Control approach. *Control Engineering Practice*, *21*(12), 1653–1664. https://doi.org/10.1016/j.conengprac.2013.09.003

Blumenschein Laura H., & Meng¨uc Yigit. (2019). *Generalized Delta Mechanisms from Soft Actuators*. IEEE.

Booth, J. W., Case, J. C., White, E. L., Shah, D. S., & Kramer-Bottiglio, R. (2018). An addressable pneumatic regulator for distributed control of soft robots. *2018 IEEE International Conference on Soft Robotics, RoboSoft 2018*, 25–30. https://doi.org/10.1109/ROBOSOFT.2018.8404892

Connolly, F., Polygerinos, P., Walsh, C. J., & Bertoldi, K. (2015). Mechanical programming of soft actuators by varying fiber angle. *Soft Robotics*, *2*(1), 26–32. https://doi.org/10.1089/soro.2015.0001

Habibian, S. (2019). *Analysis and Control of Fiber-Reinforced Elastomeric Enclosures Analysis and Control of Fiber-Reinforced Elastomeric Enclosures (FREEs) (FREEs)*. https://digitalcommons.bucknell.edu/masters_theses

Hawkes, E. W., Christensen, D. L., & Okamura, A. M. (2016). Design and implementation of a 300% strain soft artificial muscle. *Proceedings - IEEE International Conference on Robotics and Automation*, *2016-June*, 4022–4029. https://doi.org/10.1109/ICRA.2016.7487592

He, L., Tan, X., Suzumori, K., & Nanayakkara, T. (2021). A method to 3D print a programmable continuum actuator with single material using internal constraint. *Sensors and Actuators, A: Physical*, *324*. https://doi.org/10.1016/j.sna.2021.112674

Hošovský, A., Piteľ, J., Židek, K., Tóthová, M., Sárosi, J., & Cveticanin, L. (2016). Dynamic characterization and simulation of two-link soft robot arm with pneumatic muscles. *Mechanism and Machine Theory*, *103*, 98–116. https://doi.org/10.1016/j.mechmachtheory.2016.04.013

Hsieh, C.-T. (2017). *Investigation of Delta Robot 3D Printer for a Good Quality of Printing*. https://www.researchgate.net/publication/317825470

Jayant Patil SSBT, M., & P Deshmukh, I. M. (2015). *A Review Paper on Introduction of Parallel Manipulator and Control System*. www.ijert.org

Kadowaki, J., Sasaki, D., Yase, H., & Kusaka, R. (2021, March 7). Improvement of McKibben type artificial rubber muscle model based on end shape deformation. *2021 IEEE International Conference on Mechatronics, ICM 2021*. https://doi.org/10.1109/ICM46511.2021.9385626

Khan, A. H., & Li, S. (2020). Sliding Mode Control with PID Sliding Surface for Active Vibration Damping of Pneumatically Actuated Soft Robots. *IEEE Access*, *8*, 88793–88800. https://doi.org/10.1109/ACCESS.2020.2992997

Khin, P. M., Hong Kai. Yap, Marcelo H. Ang Jr, & Chen-Hua. Yeow. (2017). *Fabric-based Actuator Modules for Building Soft Pneumatic Structures with High Payload-to-Weight Ratio*. IEEE.

Liu, Q., Zuo, J., Zhu, C., & Xie, S. Q. (2020). Design and control of soft rehabilitation robots actuated by pneumatic muscles: State of the art. *Future Generation Computer Systems*, *113*, 620–634. https://doi.org/10.1016/j.future.2020.06.046

Lloyd, P., Hoshiar, A. K., da Veiga, T., Attanasio, A., Marahrens, N., Chandler, J. H., & Valdastri, P. (2020). A Learnt Approach for the Design of Magnetically Actuated Shape Forming Soft Tentacle Robots. *IEEE Robotics and Automation Letters*, *5*(3), 3937–3944. https://doi.org/10.1109/LRA.2020.2983704

Lynch Kevin. (2015). *Empirical PID gain tuning (Kevin Lynch) - YouTube*. https://www.youtube.com/watch?v=uXnDwojRb1g&t=226s

Marchese, A. D., & Rus, D. (2016). Design, kinematics, and control of a soft spatial fluidic elastomer manipulator. *International Journal of Robotics Research*, *35*(7), 840–869. https://doi.org/10.1177/0278364915587925

Meng, G. Z., Yuan, G. M., Liu, Z., & Zhang, J. (2013). Forward and inverse kinematic of continuum robot for search and rescue. *Advanced Materials Research*, *712–715*, 2290–2295. https://doi.org/10.4028/www.scientific.net/AMR.712-715.2290

Ouyang Bo, Hangjie Mo, Haoyao Chen, Yunhui Liu, & Dong Sun. (2018). *Robust Model-Predictive Deformation Control of a Soft Object by Using a Flexible Continuum Robot*. IEEE.

Poppeová Viera, Uríček Juraj, Bulej, V., & Šindler Peter. (2011). *Delta robots-robots for high speed manipulation*. https://www.researchgate.net/publication/298131573

Skorina Erik H., Ming Luo, S. O., Fuchen Chen, Weijia Tao, & Cagdas D. Onal. (2015). *Feedforward augmented Sliding Mode Motion Control of Antagonistic Soft Pneumatic Actuators*. IEEE.

Skorina Erik H., Weijia Tao, Fuchen Chen, Ming Luo, & Cagdas D. Onal. (2016). *2016 IEEE International Conference on Robotics and Automation : Stockholm, Sweden, May 16th 21st*. IEEE.

Sun, T., Chen, Y., Han, T., Jiao, C., Lian, B., & Song, Y. (2020). A soft gripper with variable stiffness inspired by pangolin scales, toothed pneumatic actuator and autonomous controller. *Robotics and Computer-Integrated Manufacturing*, *61*. https://doi.org/10.1016/j.rcim.2019.101848

Terryn, S., Brancart, J., Lefeber, D., Assche, G. van, & Vanderborght, B. (2017). Self-healing soft pneumatic robots. In *Sci. Robot* (Vol. 2). http://robotics.sciencemag.org/

Terryn, S., Langenbach, J., Roels, E., Brancart, J., Bakkali-Hassani, C., Poutrel, Q. A., Georgopoulou, A., George Thuruthel, T., Safaei, A., Ferrentino, P., Sebastian, T., Norvez, S., Iida, F., Bosman, A. W., Tournilhac, F., Clemens, F., van Assche, G., & Vanderborght, B. (2021). A review on self-healing polymers for soft robotics. In *Materials Today* (Vol. 47, pp. 187–205). Elsevier B.V. https://doi.org/10.1016/j.mattod.2021.01.009

Thierry Soriano. (2019, July 22). *Pince robot SG90 (gripper) | 3D CAD Model Library | GrabCAD*. https://grabcad.com/library/pince-robot-sg90-gripper-1

Thuruthel, T. G., Falotico, E., Renda, F., & Laschi, C. (2019). Model-Based Reinforcement Learning for Closed-Loop Dynamic Control of Soft Robotic Manipulators. *IEEE Transactions on Robotics*, *35*(1), 127–134. https://doi.org/10.1109/TRO.2018.2878318

Truby, R. L., Santina, C. della, & Rus, D. (2020). Distributed proprioception of 3d configuration in soft, sensorized robots via deep learning. *IEEE Robotics and Automation Letters*, *5*(2), 3299–3306. https://doi.org/10.1109/LRA.2020.2976320

Wang, T., Ge, L., & Gu, G. (2018). Programmable design of soft pneu-net actuators with oblique chambers can generate coupled bending and twisting motions.

Sensors and Actuators, A: Physical, *271*, 131–138. https://doi.org/10.1016/j.sna.2018.01.018

Wang, Y., & Xu, Q. (2021). Design and testing of a soft parallel robot based on pneumatic artificial muscles for wrist rehabilitation. *Scientific Reports*, *11*(1). https://doi.org/10.1038/s41598-020-80411-0

Webster, R. J., & Jones, B. A. (2010). Design and kinematic modeling of constant curvature continuum robots: A review. *International Journal of Robotics Research*, *29*(13), 1661–1683. https://doi.org/10.1177/0278364910368147

Young, T. R., Xavier, M. S., Yong, Y. K., & Fleming, A. J. (2019). *A Control and Drive System for Pneumatic Soft Robots: PneuSoRD*. https://github.com/PrecisionMechatronicsLab/PneuSoRD

Zhang Haochong, Rongyun Cao, Shlomo Zilberstein, Feng Wu, & Xiaoping Chen. (2017). *Toward Effective Soft Robot Control via Reinforcement Learning* (Y. Huang, H. Wu, H. Liu, & Z. Yin, Eds.; Vol. 10462). Springer International Publishing. https://doi.org/10.1007/978-3-319-65289-4

Zheng, G. (2020). Control of a Silicone Soft Tripod Robot via Uncertainty Compensation. *IEEE Robotics and Automation Letters*, *5*(2), 2801–2807. https://doi.org/10.1109/LRA.2020.2974714

APPENDIX

MEASURED DATA

No.	Pressure Sequence (kPa)			YZ (cm)		XZ (cm)		XY (cm)		Average Positions (cm)			Actuator Lengths (cm)		
	P1	P2	P3	Y	Z	X	Z	X	Y	X	Y	Z	l1	l2	l3
0	0	0	0	0	20	0	20	0	0	0	0	20	20	20	20
1	60	0	0	-3.8	20.8	-0.7	20.2	-0.5	-4.1	-0.6	-3.95	20.5	24	20.5	20.5
2	120	0	0	-10.4	16.9	-0.6	18.4	-0.4	-10.2	-0.5	-10.3	17.65	25.5	20.5	20.5
3	0	60	0	2	20.2	4	20.1	5.1	1.1	4.55	1.55	20.15	20.5	23.2	20.5
4	0	120	0	4	18.5	10.5	19	9.7	4.3	10.1	4.15	18.75	20.5	25	20.5
5	0	0	60	1.2	20.6	-4	20.6	-4.3	1.5	-4.15	1.35	20.6	21	20.5	23.5
6	0	0	120	4.2	17.1	-9.3	17.7	-9.3	4.1	-9.3	4.15	17.4	20	20.5	25
7	60	120	0	-0.7	19.1	8.6	19.1	10.2	-0.5	9.4	-0.6	19.1	23	25.5	20.5
8	120	60	0	-8.8	18.4	4	17.7	3.6	-9.8	3.8	-9.3	18.05	25.2	23.5	20.6
9	0	60	120	6.5	19.1	-7	19.4	-5.7	7.5	-6.35	7	19.25	20.5	23	25
10	0	120	60	7.3	19.7	4.6	18.8	5.6	7	5.1	7.15	19.25	21	25	23
11	60	0	120	1.5	18.4	-10	18.3	-9.4	0.5	-9.7	1	18.35	22.5	20.5	25.5
12	120	0	60	-9.5	15.6	-4.1	17.8	-4.3	-9.8	-4.2	-9.65	16.7	25	20.5	23.2
13	60	60	60	0	21.6	0	22.3	0	-1	0	-0.5	21.95	22.8	22.5	22.8
14	120	120	120	0	24.1	0	24.5	0	-1	0	-0.5	24.3	25.5	25	25
15	60	60	120	4	20.3	-7.6	21.7	-7	3	-7.3	3.5	21	23	22.8	25.3
16	60	120	120	7.5	22.1	-2.2	22.9	-1.5	8	-1.85	7.75	22.5	23	24.8	25.2
17	60	120	60	3	20	5.7	21.7	6	3.2	5.85	3.1	20.85	23.3	25.2	22.8
18	120	60	60	-8.2	19.8	-0.3	20	-0.3	-7.2	-0.3	-7.7	19.9	25.1	23.5	23.4
19	120	120	60	-5	20.9	4.4	22	5.1	-5.2	4.75	-5.1	21.45	25.5	25.3	23.4
20	120	60	120	-4	19.3	-8.5	20	-7.9	-4.7	-8.2	-4.35	19.65	25	22.8	25.5
21	60	60	0	-3	19.9	3.6	21	3.7	-2.6	3.65	-2.8	20.45	23	23.1	20.7
22	60	0	60	-2.5	18.5	-5.5	20.4	-5	-2.9	-5.25	-2.7	19.45	23	20.6	23.5
23	0	60	60	5.4	21	-1	23.1	-1.1	5.1	-1.05	5.25	22.05	20.8	23.5	23.5
24	120	120	0	-7.2	18	7.7	19	9	-7.4	8.35	-7.3	18.5	26.7	25.7	21.5
25	120	0	120	-8	15.2	-10.5	17.5	-10.2	-7	-10.35	-7.5	16.35	25.7	20.7	26.3
26	0	120	120	12	19	-1	18.6	-1.1	11.6	-1.05	11.8	18.8	20.8	25	25.2